Cross-section resistance and design of stainless steel CHS and EHS at elevated temperatures

Chunyan Quan, Merih Kucukler [*]

School of Engineering, University of Warwick, Coventry CV4 7AL, UK

ARTICLE INFO

ABSTRACT

The structural behaviour and design of stainless steel circular hollow sections (CHS) and elliptical hollow sections (EHS) at elevated temperatures are investigated in this paper. Shell finite element models of stainless steel CHS and EHS are created and validated against experimental results from the literature, which are subsequently used to generate benchmark structural performance data. Parametric studies are performed on a large number of cold-formed and hot-rolled austenitic, duplex and ferritic stainless steel CHS and EHS subjected to (i) pure axial compression, (ii) pure bending, (iii) combined axial compression and bending and (iv) combined bending and shear at elevated temperatures; the studied cases comprise 24,495 stainless steel CHS and EHS in fire and cover a wide range of cross-section slendernesses and elevated temperature levels. Calibrated against the benchmark structural performance data obtained from the numerical parametric studies, new design proposals for predicting the cross-section resistances of stainless steel CHS and EHS in fire are put forward. The accuracy, safety and reliability of the new design proposals are assessed. It is shown that in comparison to the design provisions of the European structural steel fire design standard EN 1993-1-2, the proposed design methods provide more accurate and safe-sided cross-section resistance predictions for stainless steel CHS and EHS at elevated temperatures.

1. Introduction

Stainless steel is increasingly being used in the construction and offshore industries owing to its excellent corrosion resistance, very high durability and low maintenance costs. In comparison to carbon steel, stainless steel also exhibits superior strength and stiffness retention at elevated temperatures [1], resulting in a considerably improved fire performance for stainless steel structures [2]. Owing to their aesthetic appearance, circular hollow sections (CHS) and elliptical hollow sections (EHS) are widely used in structural applications. Relative to open section members, CHS and EHS members also possess significantly higher torsional stiffness, which effectively suppresses flexural–torsional instabilities. Combining the structural advantages of CHS and EHS and the benefits of stainless steel as a construction material, stainless steel CHS and EHS structural members are increasingly being used in practice and their fire design is of interest to designers. However, thus far, the previous research has predominantly focused on the room temperature structural response and design of stainless steel CHS and EHS and there is very limited knowledge with respect to the behaviour and design of stainless steel CHS and EHS structural members at elevated temperatures.

Local buckling impairs the cross-section resistances of steel cross-sections, which must be considered in both room temperature and elevated temperature design. The current European structural steel fire design standard EN 1993-1-2 [3] adopts the room temperature local buckling assessment rules provided in the European room temperature structural steel standard EN 1993-1-1 [4] and stainless steel design standard EN 1993-1-4 [5] to consider the influence of local instability effects on the ultimate resistances of carbon steel and stainless steel cross-sections in fire, respectively. However, these design rules were originally developed by taking into account the local buckling response of carbon steel and stainless steel cross-sections at room temperature, thus typically providing inaccurate estimations of the structural behaviour of carbon steel and stainless steel cross-sections in fire owing to the significantly different material response of carbon steel and stainless steel at elevated temperatures. Considering this, recently, a number of research studies into the local buckling behaviour of carbon steel and stainless steel elements at elevated temperatures have been performed. Ranby [6] recommended the use of room temperature steel cross-section design methods with (i) the elevated temperature material strengths at 2% total strain $f_{2,\theta}$ for the fire design of Class 1, 2 and 3 steel

---

* Corresponding author.
   E-mail address: merih.kucukler@warwick.ac.uk (M. Kucukler).

(a) Stub columns and beam-columns

(b) Beams subjected to uniform bending

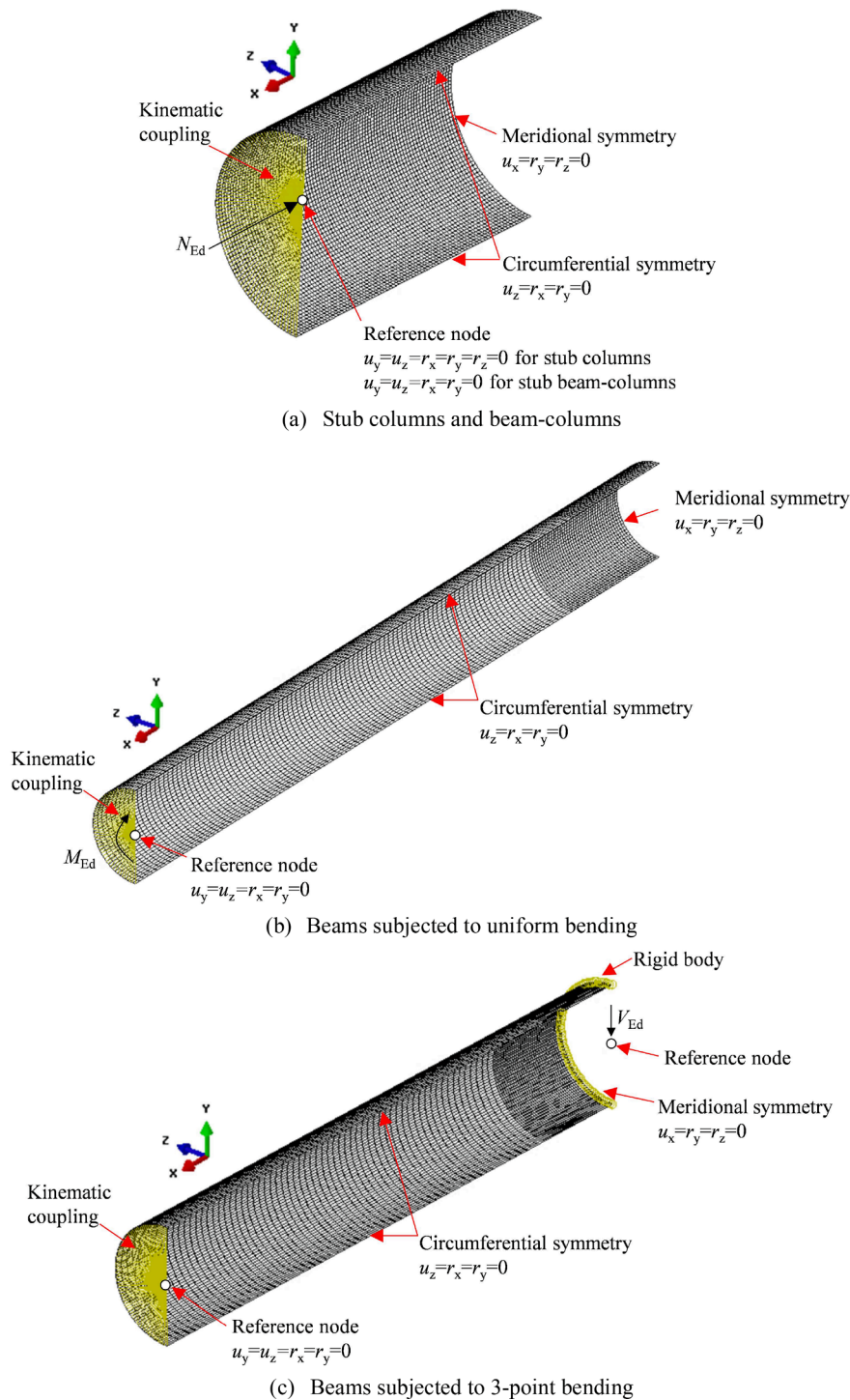(c) Beams subjected to 3-point bending

Fig. 1. Details of finite element models developed in this study.

cross-sections and (ii) the elevated temperature 0.2% proof strengths $f_{p0.2,\theta}$ for the fire design of Class 4 steel cross-sections, considering the low probability of the attainment of high strain levels in Class 4 steel cross-sections due to local buckling. This recommendation was adopted in EN 1993-1-2 [3] in conjunction with the room temperature local buckling design rules provided in EN 1993-1-1 [4] and EN 1993-1-4 [5] for the local buckling assessment of carbon steel and stainless steel cross-sections at elevated temperatures, respectively. However, [7–9] demonstrated that EN 1993-1-2 [3] does not only lead to rather inaccurate ultimate resistance predictions for steel cross-sections in fire in a large number of cases but also generates an artificial step between the

ultimate resistance predictions for Class 3 and 4 cross-sections owing to the adoption of two distinct elevated temperature material strengths (i. e. $f_{2,\theta}$ and $f_{p0.2,\theta}$). To eliminate this inaccuracy and discontinuity, Couto et al. [9] recommended the use of the elevated temperature material strengths at 2% total strain $f_{2,\theta}$ for the ultimate resistance predictions of steel cross-sections in fire regardless of their cross-section class in conjunction with a new effective width method for carbon steel plates at elevated temperatures. Considering that Couto et al. [9] only took into account the structural response of carbon steel plates and cross-sections in fire, Xing et al. [10] investigated the local buckling behaviour of stainless steel plates at elevated temperatures and proposed a new

Table 1

Determination of equivalent diameters D_e for CHS and EHS under different loading conditions.

Cross-section	Loading condition	Equivalent diameter D_e
CHS	Axial compression Bending	D
EHS	Axial compression	$D\left[1 + \left(1 - 2.3\left(\frac{t}{D}\right)^{0.6}\right)\left(\frac{D}{B} - 1\right)\right]$ or conservatively equal to $\frac{D^2}{B}$
	Major axis bending	$\frac{B^2}{D}$ for $D/B \leq 1.36$ $0.4\frac{D^2}{B}$ for D/B greater than 1.36
	Minor axis bending	$\frac{D^2}{B}$

effective width-based design method to accurately predict the ultimate resistances of stainless steel plates at elevated temperatures, employing the elevated temperature material strengths at 2% total strain $f_{2,\theta}$ as the reference material strengths in all design cases. The design approach proposed in Xing et al. [10] has also been verified for stainless steel welded I-sections subjected to pure axial compression and pure bending at elevated temperatures by [11]. However, since it was developed for the local buckling assessment of stainless steel I-sections and square and rectangular hollow sections (i.e. flat sections) at elevated temperatures, the design approach put forward in [10] cannot be used for the local buckling assessment of stainless steel CHS and EHS (i.e. non-flat sections) in fire. Taking into account the need for the accurate fire design of steel CHS elements, Kucukler [12] investigated the compressive behaviour of carbon steel CHS members at elevated temperatures and proposed a new design method which is able to provide accurate and safe compressive resistance predictions for high-strength and normal-strength carbon steel CHS at elevated temperatures. However, since carbon steel and stainless steel have distinctively different material characteristics at elevated temperatures, the design method developed in [12] is also not applicable to stainless steel CHS in fire and it is still necessary to develop a fire design method specifically for stainless steel CHS. Moreover, owing to the increasing use of stainless steel EHS members in practice [13], a new design method furnishing accurate estimations of the local buckling resistances of EHS in fire is also required, which currently does not exist in the literature.

Considering the necessity for the development of accurate fire design methods for stainless steel circular hollow sections (CHS) and elliptical hollow sections (EHS), a research study focusing on the cross-section behaviour and design of stainless steel CHS and EHS at elevated temperatures is carried out in this paper. Both cold-formed and hot-rolled CHS and EHS and austenitic, duplex and ferritic stainless steel grades are considered; a wide range of cross-section slendernesses and elevated temperature levels are covered; different loading conditions such as (i) pure axial compression, (ii) pure bending, (iii) combined compression and bending and (iv) combined bending and shear are investigated. Calibrated against the numerical results obtained from the validated shell finite element (FE) models of 24,495 stainless steel CHS and EHS in fire, new design methods for predicting the cross-section resistances of stainless steel CHS and EHS at elevated temperatures are developed.

The proposed fire design rules are also compared against the design rules provided in the European structural steel fire design standard EN 1993-1-2 [3] for the local buckling assessment of stainless steel CHS and EHS in fire. It is shown that relative to the existing EN 1993-1-2 [3] provisions, the proposed design rules provide considerably more accurate, safe and reliable ultimate resistance predictions for stainless steel CHS and EHS at elevated temperatures.

2. Finite element modelling

In this study, shell FE models are developed to mimic the behaviour of CHS and EHS at elevated temperatures. Geometrically and Materially Nonlinear Analyses with Imperfections (GMNIA) of the shell FE models are carried out to generate extensive benchmark structural performance data for CHS and EHS in fire, against which the proposed design methods could be calibrated. The development and validation of the shell FE models and comprehensive numerical parametric studies performed in this study are described in this section.

2.1. Development of finite element models

2.1.1. Modelling approach

The finite element analysis software Abaqus [14] was used to carry out the GMNIA simulations. The four-noded shell element S4R taking into account transverse shear deformations and finite membrane strains with reduced integration and a large-strain formulation, which has been successfully employed in previous studies for similar applications [11,12,15], was used to create all the models. Employing suitable boundary conditions at the midspan and along the two longitudinal edges through the member length in line with the approach adopted in [12], two symmetry planes were exploited at the midspan and along the half of the cross-section respectively, whereby computationally efficient quarter models are generated as shown in Fig. 1. The generated quarter models have been verified against the results obtained from the corresponding full models. The end displacements and rotations were linked to the reference points where the kinematic coupling and boundary conditions are applied as can be seen from Fig. 1. For stub columns, fixed end support conditions were employed by restraining all rotations r and displacements u with the exception of the longitudinal displacements at the loaded end (i.e. $u_y = u_z = r_x = r_y = r_z = 0$). For the other members subjected to bending (i.e. stub beam-columns, beams subjected to uniform bending and 3-point bending), pin-ended support conditions about the bending axis were established at the reference points by releasing the rotation about the bending axis (i.e. $u_y = u_z = r_x = r_y = 0$, but $r_z \neq 0$). In all of the models with the exception of the 3-point bending cases, the forces (i.e. concentric or eccentric axial force N_{Ed} and bending moment M_{Ed}) were applied to the reference points at the ends, while in the models subjected to 3-point bending, all degrees of freedoms at the midspan section were linked to a reference point through rigid body and a vertical load V_{Ed} was applied to the reference point at the midspan, as shown in Fig. 1 (c). A fine mesh with shell element size of $0.1\sqrt{D_e t}$ was adopted, where t is the cross-section thickness and D_e is the equivalent diameter. The equivalent diameter D_e is equal to the outer diameter D for CHS but varies for EHS under different loading conditions [16–20] as provided in Table 1, where D is the larger outer diameter and B is the smaller outer diameter. Cross-section properties of CHS and EHS are shown in Fig. 2. The element size along the member length was chosen such that the element aspect ratios were approximately equal to unity. This meshing strategy has been shown to be sufficiently refined to provide accurate estimations of the local buckling behaviour of CHS and EHS members [21,22]. This fine mesh was applied to all regions of stub columns and stub beam-columns. For long members, e.g. uniform bending cases and 3-point bending cases, the fine mesh was only applied to the midspan regions where local buckling is expected, whose lengths were taken as six times of the elastic local buckling half-wavelengths of the cross-sections; on the other hand, for the remainder of the modelled members, a coarser mesh with the element size of $0.5\sqrt{D_e t}$ was adopted in line with [22]. This meshing strategy was also used in [21,22] for CHS and EHS members, which was shown to be able to reflect the member behaviour while also maintaining good computational efficiency. The Simpson integration method was used and five integration points were employed through the thickness of the shell elements [14]. The isothermal analysis approach was adopted for all the considered CHS
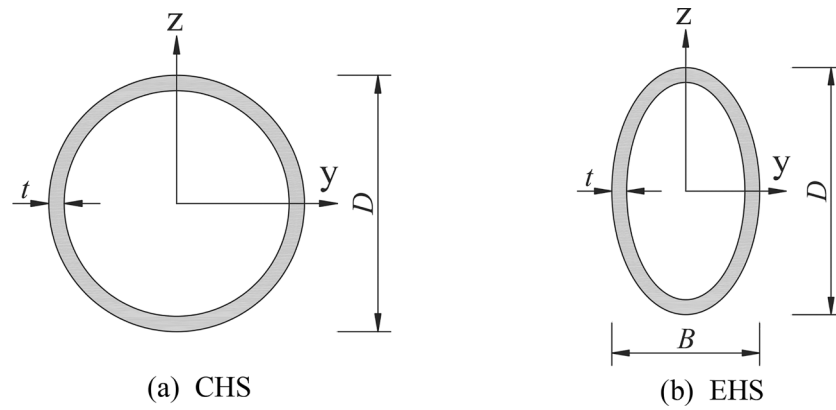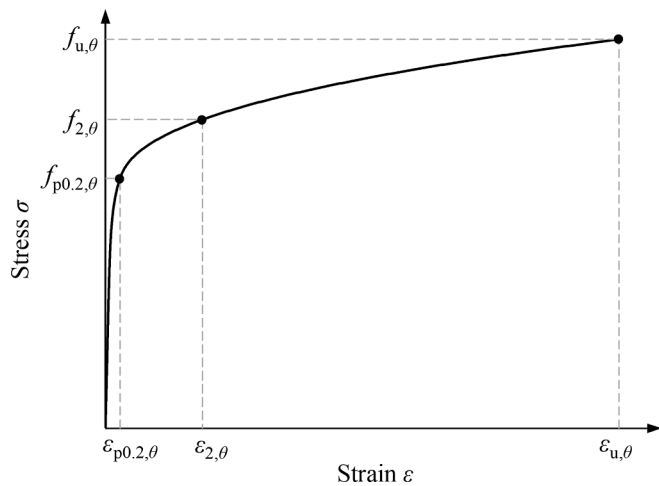
Fig. 2. Geometry of CHS and EHS.

Fig. 3. Two-stage elevated temperature Ramberg-Osgood material model for stainless steel [23–25].

and EHS in fire in this study, where the temperatures of CHS and EHS were initially increased to predefined elevated temperature levels θ which resulted in the development of thermal strains and modification of the material behaviour and then the loading was applied up to failure; the maximum values of the applied loads observed in the FE simulations were taken as the ultimate resistances of CHS and EHS at the predefined elevated temperature levels θ. The modified Riks analysis [14] was employed to obtain the full load-deformation response of the considered stainless steel CHS and EHS in all the FE simulations, including the post-ultimate response.

2.1.2. Material modelling

Both cold-formed and hot-rolled stainless steel CHS and EHS were considered in this paper. For each stainless steel family, one typical grade was chosen: 1.4301 austenitic (A), 1.4462 duplex (D) and 1.4003

ferritic (F). In this study, the two-stage Ramberg-Osgood material model [23–25] was used to express the full stress–strain σ-ε response at temperature θ, as given by Eqs. (1)-(2) and illustrated in Fig. 3, where E_θ is the Young's modulus at temperature θ, $E_{p0.2\theta}$ is the tangent modulus as given by Eq. (3), $\varepsilon_{p0.2,\theta}$ is the total strain equal to $0.002 + f_{p0.2,\theta}/E_\theta$ at the 0.2% proof stress $f_{p0.2,\theta}$, $f_{u,\theta}$ and $\varepsilon_{u,\theta}$ are the ultimate strength and strain at temperature θ and n_θ and m_θ are the strain hardening exponents, respectively. The adopted two-stage Ramberg-Osgood material model [23–25] is able to capture the nonlinear material stress–strain behaviour [26] and accurately predict the stress–strain behaviour of stainless steel at elevated temperatures [27–29]. Relative to the current provisions of EN 1993-1-2 [3], this material model is less complex but more accurate when compared to test results [28]; thus, it will be included in the up-coming version of EN 1993-1-2 [3].

$$\varepsilon = \frac{\sigma}{E_\theta} + 0.002 \left(\frac{\sigma}{f_{p0.2,\theta}} \right)^{n_\theta} \quad \text{for } \sigma \leqslant f_{p0.2,\theta} \tag{1}$$

$$\begin{aligned}
\varepsilon = \varepsilon_{p0.2,\theta} \; + \; & \frac{\sigma - f_{p0.2,\theta}}{E_{p0.2,\theta}} \\
+ & \left(\varepsilon_{u,\theta} - \varepsilon_{p0.2,\theta} - \frac{f_{u,\theta} - f_{p0.2,\theta}}{E_{p0.2,\theta}} \right) \left(\frac{\sigma - f_{p0.2,\theta}}{f_{u,\theta} - f_{p0.2,\theta}} \right)^{m_\theta} \\
& \text{for } f_{p0.2,\theta} \; < \; \sigma \leqslant f_{u,\theta}
\end{aligned} \tag{2}$$

$$E_{p0.2,\theta} = \frac{E_\theta}{1 + 0.002 n_\theta \frac{E_\theta}{f_{p0.2,\theta}}} \tag{3}$$

The material properties at elevated temperatures (i.e. $f_{p0.2,\theta}$, $f_{2,\theta}$, $f_{u,\theta}$, $\varepsilon_{u,\theta}$, E_θ) utilised in Eqs. (1)-(3) were determined by multiplying the material properties at room temperature, i.e. the yield (0.2% proof) stress f_y, ultimate stress f_u, ultimate strain ε_u and Young's modulus E by the corresponding strength ($k_{p0.2,\theta}$, $k_{2,\theta}$, $k_{u,\theta}$), ductility ($k_{\varepsilon u,\theta}$) and stiffness ($k_{E,\theta}$) reduction factors provided in the Steel Construction Institute (SCI) Design Manual for Structural Stainless Steel [30], which are based on the extensive elevated temperature material testing results reported in [27–29,31], thus $f_{p0.2} = k_{p0.2,\theta}f_y$, $f_{2,\theta} = k_{2,\theta}f_y$, $f_{u,\theta} = k_{u,\theta}f_u$,

Table 2
Summary of the adopted standardised material properties for stainless steel in the FE models [32].

Type	Grade	Young's modulus E (N/mm^2)	Yield (0.2% proof) stress f_y (N/mm^2)	Ultimate stress f_u (N/mm^2)	Ultimate strain ε_u	Strain hardening exponent n
	Austenitic (A)		460	700	0.20	7.1
Cold-formed	Duplex (D)	200,000	630	780	0.13	7.5
	Ferritic (F)		430	490	0.06	11.5
	Austenitic (A)		280	580	0.50	9.1
Hot-rolled	Duplex (D)	200,000	530	770	0.30	9.3
	Ferritic (F)		320	480	0.16	17.2

(a) CHS under compression

(b) EHS under combined compression and major axis bending

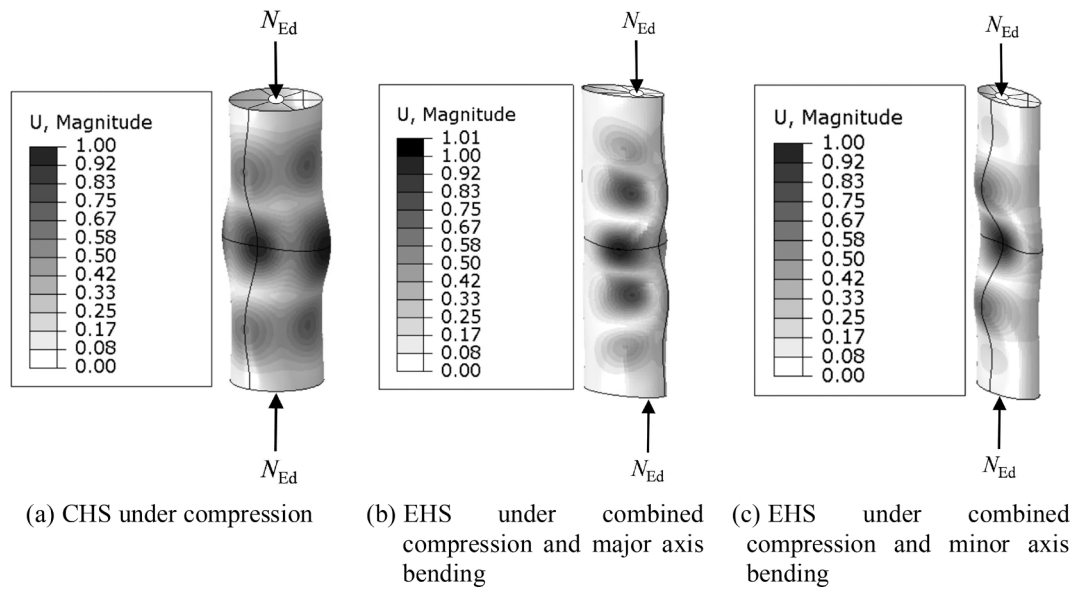(c) EHS under combined compression and minor axis bending

Fig. 4. Typical elastic local buckling modes of CHS and EHS.

Table 3
Summary of the validation study for the developed shell FE models against the experimental results from [38,13].

Reference	No. of tests	Grade	Section	Fire condition	$N_{u,FE}/N_{u,test}$			
					Mean	CoV	Max	Min
He et al. (2019) [38]	16	A	CHS	Post-fire	0.984	0.061	1.079	0.898
Theofanous et al. (2009) [13]	6	A	EHS	Room temperature	0.959	0.010	0.971	0.945

$\varepsilon_{u,\theta} = k_{\varepsilon u,\theta}\varepsilon_u$ and $E_\theta = k_{E,\theta}E$. Since the material reduction factors from the SCI Design Manual for Structural Stainless Steel [30] consider the results from a higher number of elevated temperature material tests than those taken into account in the development of EN 1993-1-2 [3], they lead to more accurate estimations of the elevated temperature material properties of different stainless steel grades. The adopted material reduction factors in this study will also be included in the upcoming version of EN 1993-1-2 [3]. The standardised room temperature material properties for stainless steel recommended in [32], which were derived based on the analysis of a comprehensive material test data on different stainless steel products existing in the literature, were employed in this study, as shown in Table 2. Note that the additional strength enhancement is gained from cold working in cold-formed steel sections [33]. In line with the recommendations of [30], the strain hardening exponent n_θ which is used to define the first stage of the elevated temperature material response was assumed as equal to the room temperature values n, which were taken from [32] and are listed in Table 2. The strain hardening exponent m_θ was calculated using Eq. (4) [34] to ensure that the second stage of the Ramberg-Osgood material model passes through $f_{2,\theta}$ and $f_{u,\theta}$ exactly at the 2% total strain and ultimate strain $\varepsilon_{u,\theta}$, respectively.

$$m_\theta = \frac{\ln\left(\frac{0.02 - \varepsilon_{p0.2,\theta} - \frac{f_{2,\theta} - f_{p0.2,\theta}}{E_{p0.2,\theta}}}{\varepsilon_{u,\theta} - \varepsilon_{p0.2,\theta} - \frac{f_{u,\theta} - f_{p0.2,\theta}}{E_{p0.2,\theta}}}\right)}{\ln\left(\frac{f_{2,\theta} - f_{p0.2,\theta}}{f_{u,\theta} - f_{p0.2,\theta}}\right)} \text{ but } 1.5 \leqslant m_\theta \leqslant 5 \quad (4)$$

2.1.3. Initial imperfections

Since this study focuses on the cross-section behaviour of stainless steel CHS and EHS in fire, only local imperfections were taken into consideration in the parametric studies. Local imperfections were incorporated into the FE models in the form of the lowest elastic local buckling modes obtained from the Linear Buckling Analyses (LBA) of the modelled sections but with a modified thickness of $t_{mod} = D/5$ for CHS

and $t_{mod} = B/5$ for EHS, where B is the smaller outer diameter of EHS; this modified approach was found to effectively preclude the use of inappropriate elastic local buckling shapes with unrealistically short local buckling half-wavelengths in the application of local geometric imperfections to the finite element models of CHS and EHS [22]. Fig. 4 presents examples of typical elastic local buckling modes obtained from LBA for (a) a CHS subjected to pure axial compression, (b) an EHS subjected to combined axial compression and major axis bending and (c) an EHS subjected to combined axial compression and minor axis bending. Following the recommendations of Annex C of EN 1993-1-5 [35], the local imperfection amplitudes were taken as 80% of the geometric fabrication tolerances given by EN 10219–2 [36] for cold-formed steel hollow sections and EN 10210–2 [37] for hot-rolled steel hollow sections. Thus, the geometric fabrication tolerance value was taken as $D/100$ but no less than 0.5 mm for CHS and EHS and it was also lower than 10 mm for CHS. Residual stresses were not incorporated into the shell FE models since their magnitudes are quite low within stainless steel CHS and EHS and become even smaller at elevated temperatures due to the development of thermal strains, thus having an insignificant influence on the cross-section behaviour in fire [12].

2.2. Validation of numerical models

The shell FE models developed in this study were validated against the results from physical experiments performed on stainless steel CHS and EHS in the literature [13,38,39]. The geometric properties, material properties, boundary conditions and loading conditions of the shell FE models were consistent with those employed in the considered experiments.

Since there is currently no experimental study performed on stainless steel CHS and EHS stub columns or beam-columns at elevated temperatures in the literature, the developed shell FE models were first validated against experimental results on (i) austenitic stainless steel CHS
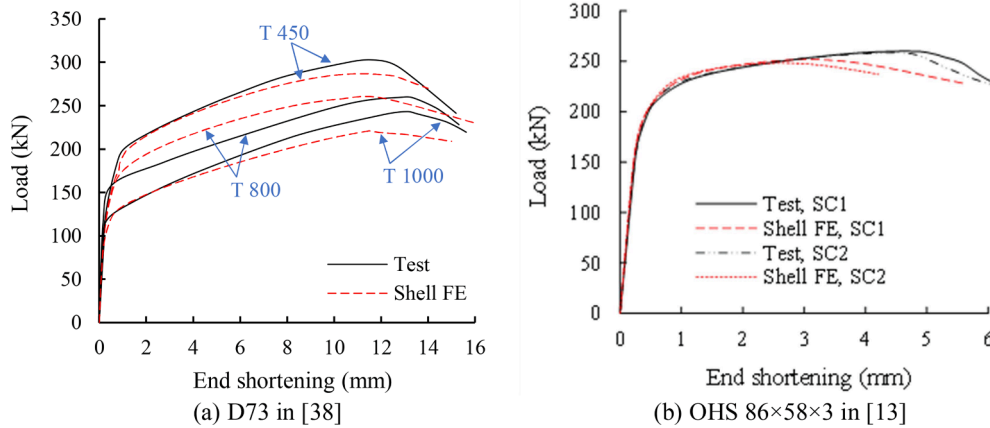
Fig. 5. Comparison of the load-end shortening paths obtained from the experiments in [38,13] and shell FE models for austenitic stainless steel CHS and EHS members.
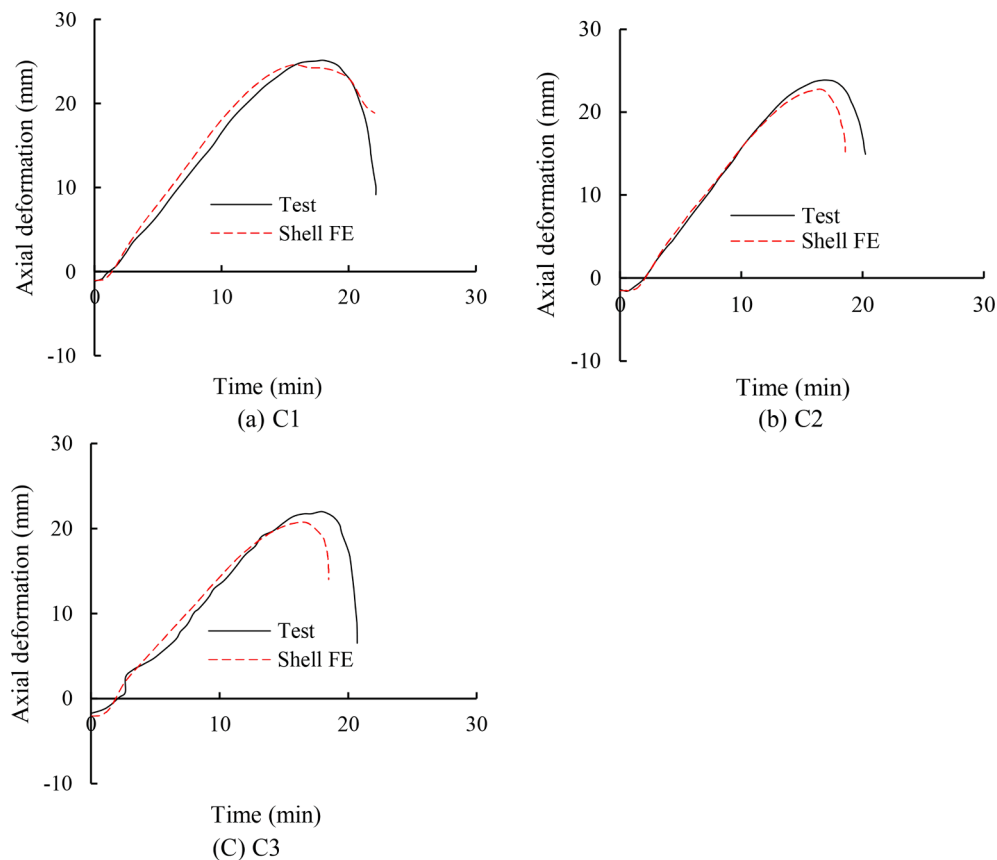

Fig. 6. Comparison of the axial deformation versus time paths obtained from the experiments in [39] and shell FE models created in this study for high strength steel CHS columns at elevated temperatures.

stub columns tested after their exposure to elevated temperatures [38] and (ii) EHS stub columns tested at room temperature [13]. Table 3 shows a summary of the validation studies against the considered experiments. In Table 3, the mean, coefficient of variation (CoV), maximum and minimum values of the ratios of the ultimate load carrying capacities determined from the shell FE models $N_{u,FE}$ to those obtained from experiments $N_{u,test}$ (i.e. $N_{u,FE}/N_{u,test}$) are provided. As can be seen from Table 3, the shell FE models created in this study are able to provide ultimate strength predictions that are generally very close to those obtained from the physical experiments of [38] and [13]. Fig. 5 presents the experimental and numerical load-deformation curves for a sample of the tested specimens. Fig. 5 (a) displays the axial load-end shortening curves of the specimens labelled as the D73 series which were tested after their exposure to the elevated temperature values of 450 °C, 800 °C and 1000 °C (referred to as T 450, T 800 and T 1000) in [38]. Moreover, Fig. 5 (b) shows the axial load-end shortening curves of the EHS specimens OHS 86 × 58 × 3-SC1 and OHS 86 × 58 × 3-SC2 tested at room temperature in [13]. It can be seen from the figures that the numerical load-deformation paths generally agree well with the experimental load-deformation paths, highlighting the ability of the developed finite element models in this study to replicate the behaviour of CHS and EHS subjected to local instability effects.

The fire experiments on pin-ended high-strength steel CHS columns performed by Tondini et al. [39] were also utilised to validate the shell FE modelling approach adopted in this study. For these long columns, in addition to the local imperfections as described in Section 2.1.3, global imperfections were also incorporated into the FE models, using the lowest global buckling modes scaled to the maximum amplitudes of 1/1000 of the member lengths L (i.e. $L/1000$). In [39], anisothermal experiments were carried out, whereby a series of predefined axial loads were first applied to the specimens, and then their temperatures were increased until failure while the applied axial loads were kept constant. The specimen temperature versus time relationships measured during the experiments were adopted in the FE analysis. Since (i) the elevated temperature material properties of the specimens were not provided in Tondini et al. [39] and (ii) the room temperature material properties of the specimens reported in [39] were close to the room temperature material properties measured for coupons made of grade S690 steel by Qiang et al. [40], in the finite element models of the specimens created herein, the elevated temperature material properties of the specimens were defined through multiplying the material reduction factors derived in [40] for S690 steel by the corresponding room temperature material properties of the specimens from [39], following the approach adopted by [12]. Comparison of the axial deformation versus time curves of the C1, C2 and C3 specimens observed in the experiments of [39] and those obtained from the shell FE models are shown in Fig. 6. As can be seen from the figures, the axial deformation-time paths obtained from the shell FE models closely follow the paths observed in the experiments. The validation studies performed in this section indicate that the shell FE models created in this paper are able to accurately replicate the structural response of CHS and EHS in fire and at room temperature and can be used to generate benchmark structural performance data for their response at elevated temperatures, against which new design methods can be calibrated. It should be noted that the adopted finite element modelling approach has also been extensively validated for stainless steel and carbon steel plates, cross-sections, columns in fire in Kucukler et al. [7,12,41,42] and Xing et al. [10,11].

2.3. Parametric studies

Upon the validation of the FE models developed in this study, parametric studies were carried out to generate benchmark structural performance data. Table 4 summaries the details of the numerical parametric studies. Both cold-formed and hot-rolled austenitic, duplex and ferritic stainless steel were considered, covering (i) stub columns subjected to pure axial compression N_{Ed}, (ii) beams subjected to uniform bending M_{Ed} ($M_{y,Ed}$ for major axis bending or $M_{z,Ed}$ for minor axis bending), (iii) stub beam-columns subjected to combined axial compression N_{Ed} and major or minor axis bending M_{Ed}, and (iv) beams subjected to major or minor axis 3-point bending which leads to combined bending M_{Ed} and shear V_{Ed}. Isothermal analyses were performed for all the considered members, adopting five different elevated temperature levels of $\theta = 300\,°C$, $400\,°C$, $500\,°C$, $600\,°C$ and $700\,°C$. The aspect ratios of the studied EHS, i.e. the ratios of the larger outer diameter D to the smaller outer diameter B, were taken as $D/B = 1.5$, 2 and 2.5. The outer diameter D of CHS and the larger outer diameter D of EHS were taken as a contant value equal to 100 mm in all the considered cases in the numerical parametric studies, while the cross-section thicknesses t were varied to achieve a broad spectrum of cross-section slendernesses for CHS and EHS in fire. To take into account the influence of different material strengths on the local buckling behaviour of CHS and EHS, the normalised material strength factor ($f_y/235$) was adopted in the consideration of varying cross-section thicknesses in the parametric studies, considering the use of this normalised material strength factor ($f_y/235$) in the cross-section classification rules of EN 1993-1-1 [4] and EN 1993-1-4 [5]. For CHS subjected to pure axial compression and pure bending, the diameter D to cross-section thickness t ratios multiplied by ($f_y/235$) were ranged between 20 and 250 with an

Table 4
Summary of parametric studies performed on stainless steel CHS and EHS at elevated temperatures.

Cross-section	Material	θ (°C)	D/B	$(D_e t/t)(f_y/235)$					L/D		
				N_{Ed}	M_{Ed}	$N_{Ed}+M_{Ed}$	$M_{Ed}+V_{Ed}$	N_{Ed}	M_{Ed}	$N_{Ed}+M_{Ed}$	$M_{Ed}+V_{Ed}$
CHS	Cold-formed and hot-rolled	300 400 500 600 700	1	20 – 250 with Δ10	20 – 250 with Δ10	20 – 240 with Δ20	20 – 100 with Δ10	3	$7\sqrt{\dfrac{D}{8t}}$	3	2, 3, 5, 10
EHS	A D F		1.5 2 2.5	40 – 250 with Δ10	40 – 250 with Δ10	*40 – 240 with Δ20	$(D/t)(f_y/235)=20-100$ with Δ10 (major axis) $(B/t)(f_y/235)=20-100$ with Δ10 (minor axis)		$7\sqrt{\dfrac{D}{8t}}$ (major axis) $7\sqrt{\dfrac{B}{8t}}$ (minor axis)		$L/D=$ 2, 3, 5, 10 (major axis) $L/B=$ 2, 3, 5, 10 (minor axis)

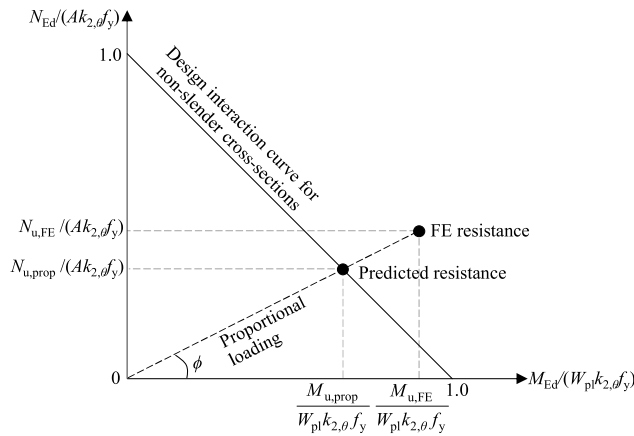* D_e is the equivalent diameter of EHS under pure axial compression (see Table 1).

Fig. 7. Definition of radial angle ϕ for the combined compression and bending loading condition.

Table 5
Limit equivalent diameter D_e to thickness t ratios $(D_e/t)_{lim}$ for the classification of stainless steel CHS and EHS at elevated temperatures according to EN 1993-1-2 [3].

Class	Compression	Bending
Class 1	$(D_e/t)_{lim} = 50\varepsilon_\theta^2$	$(D_e/t)_{lim} = 50\varepsilon_\theta^2$
Class 2	$(D_e/t)_{lim} = 70\varepsilon_\theta^2$	$(D_e/t)_{lim} = 70\varepsilon_\theta^2$
Class 3	$(D_e/t)_{lim} = 90\varepsilon_\theta^2$	$(D_e/t)_{lim} = 280\varepsilon_\theta^2$

increment of 10 (i.e. $(D/t)(f_y/235) = 20$–250 with $\Delta 10$). While for EHS subjected to pure axial compression and pure bending, $(D_e/t)(f_y/235)$ ratios were ranged between 40 and 250 with an increment of 10; note that a higher lower limit was adopted for $(D_e/t)(f_y/235)$ ratios in the case of EHS to avoid unrealistic thicknesses for high cross-section aspect ratios D/B. For CHS and EHS under combined bending and axial compression, $(D_e/t)(f_y/235)$ ratios were ranged between 20 and 240 and 40–240 with an increment of 20. In the case of CHS subjected to 3-point bending (i.e. combined bending and shear), $(D/t)(f_y/235)$ ratios were ranged between 20 and 100 with an increment of 10; while for EHS subjected to major and minor axis 3-point bending, $(D/t)(f_y/235)$ and $(B/t)(f_y/235)$ were ranged between 20 and 100 with an increment of 10, respectively. As can be seen from Table 4, to avoid the cases where shear buckling may be of significance, an upper limit of 100 is imposed on $(D/t)(f_y/235)$ and $(B/t)(f_y/235)$ ratios for CHS and EHS under 3-point bending (i.e. combined bending and shear), considering the recommendations of [43]. The shear buckling of CHS and EHS in fire will be comprehensively investigated in future research and is outside the scope of this study. It should be noted that in EN 1993-1-4 [5], the nominal thicknesses of cold-formed cross-sections is limited to 6.4 mm or 8 mm for different stainless steel grades. Thus, the cross-section thicknesses of the studied cold-formed CHS and EHS are limited to 6 mm in the numerical parametric studies in line with [2,44].

As summarised in Table 4, for stub columns and stub beam-columns, the member length L was taken as three times of the cross-section depth $3D$ in accordance with [45], which is deemed long enough for free development of local buckling but also short enough to avoid significant influence from global buckling. For CHS members subjected to 3-point bending and EHS members subjected to 3-point major axis bending, the member length to cross-section depth L/D ratios were taken as 2, 3, 5, and 10, while for EHS members subjected to 3-point minor axis bending, the member length to cross-section width L/B ratios were taken as 2, 3, 5, and 10 whereby different interaction levels of bending and shear could be captured. For the case of CHS and EHS subjected to pure bending, the bending capacity may be influenced by the member length due to the ovalisation effect [46,47]. To account for the ovalisation

effect, the member length in uniform bending should be long enough, which was taken as $L = 7D\sqrt{D/8t}$ for CHS and EHS subjected major axis bending and $L = 7D\sqrt{B/8t}$ for EHS subjected to minor axis bending. These adopted member lengths correspond to the long cylinder domain in which the ovalisation effect is stable and essentially the most severe [46,47].

For CHS and EHS stub beam-columns, which are subjected to combined axial compression and major or minor axis bending, a parameter referred to as the radial angle ϕ was used to describe the level of interaction between the applied axial compression N_{Ed} and bending moment M_{Ed}, as determined by Eq. (5) and presented in Fig. 7. In Eq. (5), A and W_{pl} are the cross-section area and plastic section modulus, respectively.

$$\phi = \tan^{-1}\left(\frac{N_{Ed}/(Ak_{2,\theta}f_y)}{M_{Ed}/(W_{pl}k_{2,\theta}f_y)}\right) \tag{5}$$

As shown in Fig. 7, the radial angle ϕ varies between 0° and 90°. In this study, in addition to pure bending $\phi = 0°$ and pure axial compression $\phi = 90°$, five different radial angles $\phi = 15°, 30°, 45°, 60°$ and 75° were also considered in the numerical analyses of stub beam-columns in fire, thereby accounting for different intensity levels for axial compression and bending.

Taking into consideration the broad range of parameters shown in Table 4, in total, 24,495 stainless steel CHS and EHS members at elevated temperatures were considered in the numerical parametric studies in this paper, which comprised (i) 2500 CHS and EHS stub columns, (ii) 4475 CHS and EHS subjected to uniform bending, (iii) 10,600 CHS and EHS stub beam-columns subjected to combined axial compression and bending and (iv) 6920 CHS and EHS beams subjected to three-point bending which resulted in the application of combined shear and bending. The comprehensive structural performance data obtained from these extensive numerical parametric studies on 24,495 CHS and EHS in fire will be utilised in the following sections for the assessment of EN 1993-1-2 [3] and the development of new design methods for CHS and EHS subjected to different loading conditions at elevated temperatures.

3. EN 1993-1-2 design method for stainless steel CHS and EHS in fire

In this section, the methods provided in the European structural steel fire design standard EN 1993-1-2 [3] for the design of stainless steel CHS and EHS at elevated temperatures are briefly introduced; the accuracy of these methods is investigated in Section 5. According to EN 1993-1-2 [3], the ultimate cross-section resistances of stainless steel CHS and EHS at elevated temperatures could be calculated through the combination of the general fire design rules given in EN 1993-1-2 [3] and the room temperature design rules given in the European room temperature structural stainless EN 1993-1-4 [5] and carbon steel EN 1993-1-1 [4] design standards, adopting the elevated temperature material properties of stainless steel. Currently, EN 1993-1-4 [5] and EN 1993-1-1 [4] do not include any provisions for the cross-section classification of steel EHS. Thus, the room temperature cross-section classification rules provided in EN 1993-1-4 [5] for CHS were adopted for the cross-section classification of EHS in this study, utilising the equivalent diameter D_e (see Table 1) in lieu of the outer diameter D specified for CHS. Note that this procedure is in line with the upcoming version of EN 1993-1-4 [5]. Moreover, EN 1993-1-4 [5] and EN 1993-1-1 [4] also does not include any design equations for the determination of the effective section properties of steel CHS and EHS. Considering this, the formulae for the determination of the effective cross-section areas A_{eff} and section moduli W_{eff} of CHS and EHS put forward in Chan and Gardner [16,17] were employed in this paper in conjunction with the provisions of EN 1993-1-2 [3] for the local buckling assessment of stainless steel CHS and EHS in fire. Note that the formulae provided in Chan and Gardner [16,17] for

Table 6
Cross-section resistances of stainless steel CHS and EHS at elevated temperature according to EN 1993-1-2 [3].

Class	Compression	Bending
Class 1 and 2	$N_{\mathrm{fi,t,Rd}} = A k_{2,\theta} f_y / \gamma_{\mathrm{M,fi}}$	$M_{\mathrm{fi,t,Rd}} = W_{\mathrm{pl}} k_{2,\theta} f_y / \gamma_{\mathrm{M,fi}}$
Class 3	$N_{\mathrm{fi,t,Rd}} = A k_{2,\theta} f_y / \gamma_{\mathrm{M,fi}}$	$M_{\mathrm{fi,t,Rd}} = W_{\mathrm{el}} k_{2,\theta} f_y / \gamma_{\mathrm{M,fi}}$
Class 4	$N_{\mathrm{fi,t,Rd}} = A_{\mathrm{eff}} k_{\mathrm{p0.2},\theta} f_y / \gamma_{\mathrm{M,fi}}$	$M_{\mathrm{fi,t,Rd}} = W_{\mathrm{eff}} k_{\mathrm{p0.2},\theta} f_y / \gamma_{\mathrm{M,fi}}$

the determination of the effective cross-section areas A_{eff} and section moduli W_{eff} of CHS and EHS will be included in the next revision of the European structural stainless steel design standard EN 1993-1-4 [5]. It is also noteworthy that the described approach used in this study in the investigation of the accuracy of EN 1993-1-2 [3] for stainless steel CHS and EHS in fire was also adopted in Martins et al. [48].

3.1. Cross-section classification

According to EN 1993-1-2 [3], the cross-section classification of stainless steel CHS and EHS in fire can be carried out following the same rules provided in the European room temperature stainless steel design standard (i.e. EN 1993-1-4 [5]) but with a reduced elevated temperature material factor ε_θ determined as given by Eq. (6) where ε is the room temperature material factor.

$$\varepsilon_\theta = 0.85\varepsilon = 0.85\sqrt{\frac{235}{f_y}\frac{E}{210000}} \tag{6}$$

In accordance with EN 1993-1-4 [5], stainless steel CHS and EHS in fire are classified into four classes, depending on the ratio of the equivalent diameter D_{e} to thickness t (i.e. D_{e}/t) as well as the elevated temperature material factor ε_θ. The limit equivalent diameter to thickness $(D_{\mathrm{e}}/t)_{\mathrm{lim}}$ ratios for CHS and EHS subjected to different loading conditions at elevated temperatures given by EN 1993-1-2 [3] are listed in Table 5. Note that the equivalent diameter D_{e} of a cross-section is calculated as shown in Table 1 for the corresponding loading condition.

3.2. Cross-section resistance

Table 6 summarises the design resistance calculations given in EN 1993-1-2 [3] for stainless steel CHS and EHS subjected to axial compression or bending at elevated temperatures on the basis of their cross-section class. In the table, $N_{\mathrm{fi,t,Rd}}$ and $M_{\mathrm{fi,t,Rd}}$ are the design axial compression and bending moment resistances of a cross-section for temperature θ at time t, A and A_{eff} are gross and effective section areas, W_{pl}, W_{el} and W_{eff} are plastic, elastic and effective section moduli and $\gamma_{\mathrm{M,fi}}$ is the partial safety factor for fire design taken as equal to unity. In line with the recommendations of Chan and Gardner [16,17], the effective section area A_{eff} and effective section modulus W_{eff} are determined using the following equations:

$$A_{\mathrm{eff}} = A\sqrt{\frac{90}{D_{\mathrm{e}}/t}\frac{235}{f_y}} \tag{7}$$

$$W_{\mathrm{eff}} = W_{\mathrm{el}}\sqrt[4]{\frac{140}{D_{\mathrm{e}}/t}\frac{235}{f_y}} \tag{8}$$

where the equivalent diameter D_{e} of a cross-section is calculated as shown in Table 1, considering the applied loading conditions. Note that according to EN 1993-1-2 [3], the effective section properties stainless steel cross-sections at elevated temperatures should be taken as the same as those for room temperature. Since the elevated temperature strength at 2% total strain $f_{2,\theta} = k_{2,\theta} f_y$ is used as the reference material strength for Class 1, 2 and 3 cross-sections but the elevated temperature 0.2% proof strength $f_{\mathrm{p0.2},\theta} = k_{\mathrm{p0.2},\theta} f_y$ is used as the reference material strength for Class 4 cross-sections, there is an artificial step between the ultimate

resistances of Class 3 and Class 4 CHS and EHS in fire according to EN 1993-1-2 [3]. The accuracy of the fire design rules provided in EN 1993-1-2 [3] for CHS and EHS is assessed in Section 5.

In the case of stainless steel CHS and EHS subjected to combined axial compression and bending, there are no specific expressions in EN 1993-1-2 [3] for the cross-section design, which can instead be treated as an extreme case of member design. Since it was assumed that stub beam-columns are not susceptible to global buckling (e.g. flexural buckling or lateral-torsional buckling) and no global imperfection was incorporated into the shell FE models in this study, the global buckling reduction factors were taken equal to unity and only the interaction between the cross-section axial compression resistance and bending resistance was taken into account in the assessment of EN 1993-1-2 [3] for the design of CHS and EHS subjected to combined axial compression and bending in fire. The design formula provided in EN 1993-1-2 [3] for cross-sections subjected to combined compression and bending at elevated temperatures is given by Eq. (9),

$$\frac{N_{\mathrm{Ed}}}{N_{\mathrm{fi,t,Rd}}} + \frac{k_y M_{y,\mathrm{Ed}}}{M_{y,\mathrm{fi,t,Rd}}} + \frac{k_z M_{z,\mathrm{Ed}}}{M_{z,\mathrm{fi,t,Rd}}} \leqslant 1 \tag{9}$$

in which $M_{y,\mathrm{Ed}}$ and $M_{z,\mathrm{Ed}}$ are the applied major and minor axis bending moments and $M_{y,\mathrm{fi,t,Rd}}$ and $M_{z,\mathrm{fi,t,Rd}}$ are the design major and minor axis bending resistances, respectively. In Eq. (9), k_y and k_z are the interaction factors as given by Eqs. (10) and (11), where the major and minor axis equivalent uniform moment factors $\beta_{\mathrm{M,y}}$ and $\beta_{\mathrm{M,z}}$ are equal to 1.1 for uniform bending moment. Note that since global buckling was not considered herein, $\bar{\lambda}_{y,\theta}$ and $\bar{\lambda}_{z,\theta}$ were taken equal to the extreme value of 0 in the determination of the cross-section resistances of CHS and EHS under combined compression and bending according to EN 1993-1-2 [3] in this study.

$$k_y = 1 - \frac{\mu_y N_{\mathrm{Ed}}}{N_{\mathrm{fi,t,Rd}}} \leqslant 3,$$
with $\mu_y = (2\beta_{\mathrm{M,y}} - 5)\bar{\lambda}_{y,\theta} + 0.44\beta_{\mathrm{M,y}} + 0.29 \leqslant 0.8$ $\qquad(10)$

$$k_z = 1 - \frac{\mu_z N_{\mathrm{Ed}}}{N_{\mathrm{fi,t,Rd}}} \leqslant 3,$$
with $\mu_z = (1.2\beta_{\mathrm{M,z}} - 3)\bar{\lambda}_{z,\theta} + 0.71\beta_{\mathrm{M,z}} - 0.29 \leqslant 0.8$ $\qquad(11)$

High shear forces have an adverse effect on the cross-section resistances of CHS and EHS at elevated temperatures, which should be taken into account in their fire design. Directing the designer to the European room temperature structural steel design standard EN 1993-1-1 [4], the European structural steel fire design standard EN 1993-1-2 [3] recommends the determination of the reduced cross-section bending resistances due to high shear forces by means of the reduced elevated temperature material strengths $f_{y,\theta,\mathrm{r}}$ as calculated by Eq. (12), where $k_{y,\theta}$ is equal to $k_{2,\theta}$ for Class 1, 2 and 3 cross-sections and $k_{\mathrm{p0.2},\theta}$ for Class 4 cross-sections.

$$f_{y,\theta,\mathrm{r}} = (1 - \rho_{\mathrm{v}})k_{y,\theta}f_y \tag{12}$$

In Eq. (12), ρ_{v} is a reduction factor for the consideration of high shear forces. The factor ρ_{v} can be calculated as given by Eq. (13) for CHS and EHS when the applied shear force V_{Ed} exceeds half of the elevated temperature plastic shear capacity $V_{\mathrm{fi,t,Rd}}$ (i.e. $V_{\mathrm{Ed}} > 0.5V_{\mathrm{fi,t,Rd}}$). The elevated temperature plastic shear resistance $V_{\mathrm{fi,t,Rd}}$ of a cross-section can be calculated using Eq. (14), in which A_{v} is the shear area. EN 1993-1-2 [3] refers to EN 1993-1-1 [4] which provides a formula for the determination of the shear areas A_{v} of CHS that is given by Eq. (15); the formulae for the determination of the shear areas A_{v} of EHS put forward in Gardner et al. [49] which will be incorporated into the upcoming version of EN 1993-1-1 [4] are also given by Eq. (16). It should be noted that the described approach of using reduced elevated temperature material strengths recommended in EN 1993-1-2 [3] in the ultimate strength predictions of CHS and EHS under high shear forces in fire is in

Table 7

Proposed factors for the determination of the effective cross-section areas A_{eff} of stainless steel CHS and EHS under compression at elevated temperatures.

Cross-section	Grade	η	β	φ
CHS	A	0.4	1.0	0.6
	D	0.4	1.0	0.7
	F	0.3	0.8	0.9
EHS	A	0.4	0.8	0.6
	D	0.4	0.8	0.7
	F	0.3	0.7	0.9

Table 8

Proposed factors for the determination of the effective section moduli W_{eff} of stainless steel CHS and EHS under bending at elevated temperatures.

Cross-section	Grade	η	β	φ
CHS	A	0.40	1.0	0.75
	D	0.40	1.0	0.85
	F	0.35	1.0	1.00
EHS (major axis)	A	0.40	1.0	0.55
	D	0.40	1.0	0.65
	F	0.35	1.0	0.85
EHS (minor axis)	A	0.40	1.0	0.80
	D	0.40	1.0	0.85
	F	0.40	1.0	0.90

accordance with the conventional approach of considering high shear effects on the ultimate resistances of structural steel members at room temperature.

$$\rho_{\text{v}} = \left(2V_{\text{Ed}}\big/V_{\text{fi,t,Rd}} - 1\right)^2 \text{ for } V_{\text{Ed}}\big/V_{\text{fi,t,Rd}} > 0.5 \tag{13}$$

$$V_{\text{fi,t,Rd}} = A_{\text{v}}k_{2,\theta}f_{\text{y}} \tag{14}$$

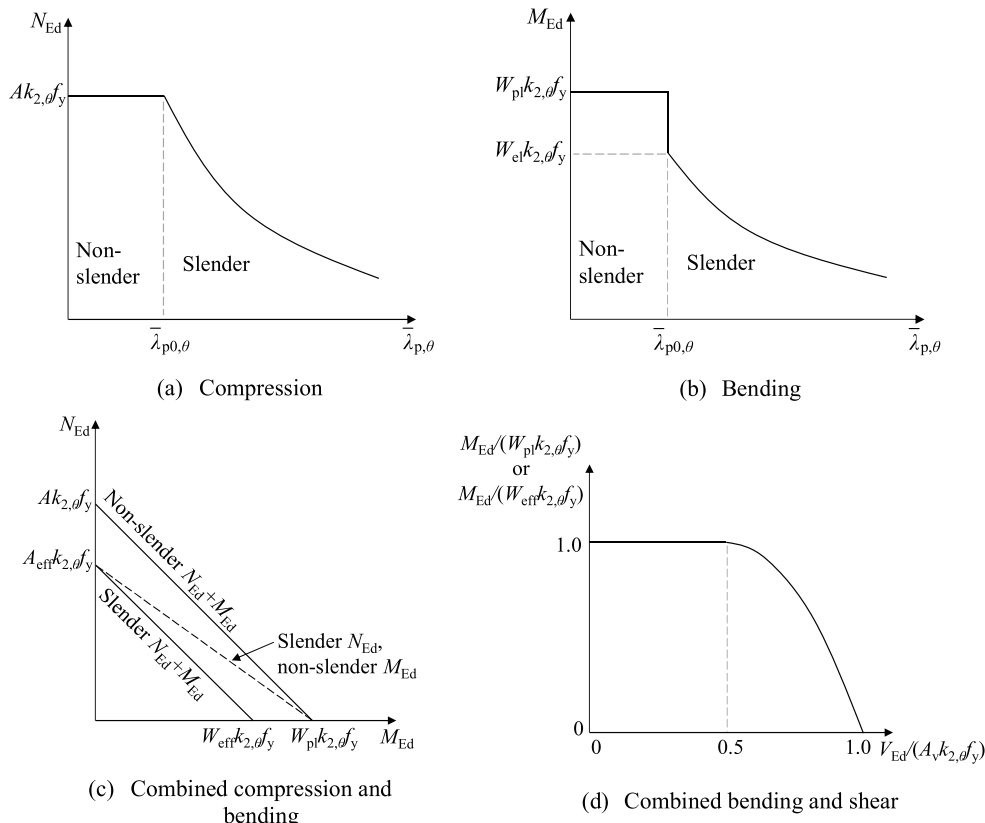$$A_{\text{v}} = 2A/\pi \text{ for CHS} \tag{15}$$

$$A_{\text{v}} = \begin{cases} 2t(D - t) & \text{for EHS under major axis bending (load parallel to depth)} \\ 2t(B - t) & \text{for EHS under minor axis bending (load parallel to width)} \end{cases} \tag{16}$$

4. Proposals for design of CHS and EHS in fire

The proposed design rules for the determination of the ultimate cross-section resistances of stainless steel CHS and EHS at elevated temperatures are presented in this section.

4.1. Cross-section classification and design at elevated temperatures

In line with (i) the design approach put forward in [10,11] for stainless steel plates and I-sections in fire and (ii) the design method developed in [12] for carbon steel CHS members at elevated temperatures, the adoption of the elevated temperature material strengths at 2% total strain $f_{2,\theta} = k_{2,\theta}f_{\text{y}}$ is recommended as the reference material strengths for the determination of the ultimate cross-section resistances of CHS and EHS in fire regardless of their cross-section class in this study. On the basis of their cross-section slenderness at elevated temperatures $\bar{\lambda}_{\text{p},\theta}$, this study recommends the classification of CHS and EHS into two classes referred to as (i) 'non-slender' and (ii) 'slender' in fire, departing from the four-class cross-section classification system given in EN 1993-1-4 [5] for room temperature design. Note that this new proposal made herein is fully in accordance with the new stainless steel fire cross-section classification rules put forward in Xing et al. [10] which will be incorporated into the upcoming version of EN 1993-1-2 [3] for the fire design of stainless steel sections.

(a) Compression

(b) Bending

(c) Combined compression and bending

(d) Combined bending and shear

Fig. 8. Proposed design cross-section resistances for stainless steel CHS and EHS at elevated temperatures under different loading conditions.

Table 9

Determination of the ultimate cross-section axial compression and bending moment resistances of stainless steel CHS and EHS at elevated temperatures according to the proposed fire design rules in this study.

Classification	Compression	Bending
Non-slender	$N_{\mathrm{fi,t,Rd}} = A k_{2,\theta} f_{\mathrm{y}} / \gamma_{\mathrm{M,fi}}$	$M_{\mathrm{fi,t,Rd}} = W_{\mathrm{pl}} k_{2,\theta} f_{\mathrm{y}} / \gamma_{\mathrm{M,fi}}$
Slender	$N_{\mathrm{fi,t,Rd}} = A_{\mathrm{eff}} k_{2,\theta} f_{\mathrm{y}} / \gamma_{\mathrm{M,fi}}$	$M_{\mathrm{fi,t,Rd}} = W_{\mathrm{eff}} k_{2,\theta} f_{\mathrm{y}} / \gamma_{\mathrm{M,fi}}$

In the proposed cross-section classification approach for CHS and EHS in fire, when the elevated temperature cross-section slenderness $\bar{\lambda}_{\mathrm{p},\theta}$ of a cross-section is lower than or equal to the threshold slenderness $\bar{\lambda}_{\mathrm{p}0,\theta}$ (i.e., $\bar{\lambda}_{\mathrm{p},\theta} \leqslant \bar{\lambda}_{\mathrm{p}0,\theta}$), the cross-section is classified as a 'non-slender' cross-section. On the other hand, if the elevated temperature cross-section slenderness of a cross-section is larger than the threshold slenderness (i.e., $\bar{\lambda}_{\mathrm{p},\theta} > \bar{\lambda}_{\mathrm{p}0,\theta}$), the cross-section is categorised as a 'slender' cross-section, for which the effective cross-section properties should be used to determine the cross-section resistance. The elevated temperature cross-section slenderness $\bar{\lambda}_{\mathrm{p},\theta}$ of CHS and EHS in fire is determined by Eq. (17),

$$\bar{\lambda}_{\mathrm{p},\theta} = \xi_\theta \sqrt{\frac{f_{\mathrm{y}}}{\sigma_{\mathrm{cr}}}} \text{ with } \xi_\theta = \sqrt{\frac{k_{2,\theta}}{k_{\mathrm{E},\theta}}} \tag{17}$$

where ξ_θ is the elevated temperature strength-to-stiffness reduction ratio factor, f_{y} is the room temperature 0.2% proof strength $f_{\mathrm{p}0.2}$, and σ_{cr} is the elastic critical local buckling stress of CHS and EHS at room temperature as determined by Eq. [50–53], in which D_{e} is the equivalent diameter of the cross-section for the corresponding loading condition as provided in Table 1 and υ is the Poisson's ratio equal to 0.3.

$$\sigma_{\mathrm{cr}} = \frac{E}{\sqrt{3(1 - \nu^2)}} \frac{2t}{D_{\mathrm{e}}} \tag{18}$$

The threshold slenderness $\bar{\lambda}_{\mathrm{p}0,\theta}$ used in the cross-section classification of CHS and EHS in fire is calculated as

$$\bar{\lambda}_{\mathrm{p}0,\theta} = \left(\eta - 0.2\sqrt{235/f_{\mathrm{y}}} \right) \sqrt{\xi_\theta} \tag{19}$$

in which η is the auxiliary coefficient; the recommended values of η for austenitic, duplex and ferritic CHS and EHS in fire are given in Table 7 and Table 8 for axial compression and bending, respectively.

4.2. Cross-section resistances of CHS and EHS under pure axial compression in fire

Design cross-section axial compression resistances $N_{\mathrm{fi,t,Rd}}$ of CHS and EHS for temperature θ at time t can be determined through Eqs. (20) and (21),

$$N_{\mathrm{fi,t,Rd}} = \frac{A k_{2,\theta} f_{\mathrm{y}}}{\gamma_{\mathrm{M,fi}}} \text{ for non-slender sections with } \bar{\lambda}_{\mathrm{p},\theta} \leqslant \bar{\lambda}_{\mathrm{p}0,\theta} \tag{20}$$

$$N_{\mathrm{fi,t,Rd}} = \frac{A_{\mathrm{eff}} k_{2,\theta} f_{\mathrm{y}}}{\gamma_{\mathrm{M,fi}}} \text{ for slender sections with } \bar{\lambda}_{\mathrm{p},\theta} > \bar{\lambda}_{\mathrm{p}0,\theta} \tag{21}$$

where A is the full cross-section area and A_{eff} is the effective cross-section area which can be calculated by Eq. (22),

$$A_{\mathrm{eff}} = \rho A \tag{22}$$

In Eq. (22), ρ is the local buckling reduction factor determined by Eq. (23), where β and φ are the auxiliary coefficients which are provided in Table 7 for austenitic, duplex and ferritic stainless steel CHS and EHS subjected to axial compression in fire.

$$\rho = 1.0 \text{ for } \bar{\lambda}_{\mathrm{p},\theta} \leqslant \bar{\lambda}_{\mathrm{p}0,\theta}$$

$$\rho = 1 - \beta \left(\frac{\bar{\lambda}_{\mathrm{p},\theta} - \bar{\lambda}_{\mathrm{p}0,\theta}}{\sqrt{\xi_\theta}} \right)^\varphi \text{ for } \bar{\lambda}_{\mathrm{p},\theta} > \bar{\lambda}_{\mathrm{p}0,\theta} \tag{23}$$

The determination of the design cross-section axial compression resistances $N_{\mathrm{fi,t,Rd}}$ of CHS and EHS for temperature θ at time t is also shown in Fig. 8 (a) and Table 9. The elevated temperature cross-section slenderness $\bar{\lambda}_{\mathrm{p},\theta}$ and the threshold slenderness $\bar{\lambda}_{\mathrm{p}0,\theta}$ for pure axial compression are calculated through Eqs. (17) and (19) respectively, employing the auxiliary coefficients η provided in Table 7 for the determination of the threshold slenderness $\bar{\lambda}_{\mathrm{p}0,\theta}$. It should be noted that unlike EN 1993-1-2 [3], this study recommends the adoption of the elevated temperature cross-section slenderness $\bar{\lambda}_{\mathrm{p},\theta}$ for the determination of the local buckling reduction factors ρ for stainless steel CHS and EHS in fire as can be seen in Eq. (23). This enables the consideration of the differential erosions of the strength and stiffness of stainless steel at different elevated temperature levels, thereby leading to the accurate assessment of the structural response of stainless steel CHS and EHS in fire.

4.3. Cross-section resistances of CHS and EHS under pure bending in fire

In accordance with the approach put forward for the local buckling assessment of CHS and EHS under pure axial compression in fire, this study recommends the determination of the design cross-section bending moment resistances $M_{\mathrm{fi,t,Rd}}$ of CHS and EHS for temperature θ at time t through Eq. (24) and (25).

$$M_{\mathrm{fi,t,Rd}} = \frac{W_{\mathrm{pl}} k_{2,\theta} f_{\mathrm{y}}}{\gamma_{\mathrm{M,fi}}} \text{ for non-slender sections with } \bar{\lambda}_{\mathrm{p},\theta} \leqslant \bar{\lambda}_{\mathrm{p}0,\theta} \tag{24}$$

$$M_{\mathrm{fi,t,Rd}} = \frac{W_{\mathrm{eff}} k_{2,\theta} f_{\mathrm{y}}}{\gamma_{\mathrm{M,fi}}} \text{ for slender sections with } \bar{\lambda}_{\mathrm{p},\theta} > \bar{\lambda}_{\mathrm{p}0,\theta} \tag{25}$$
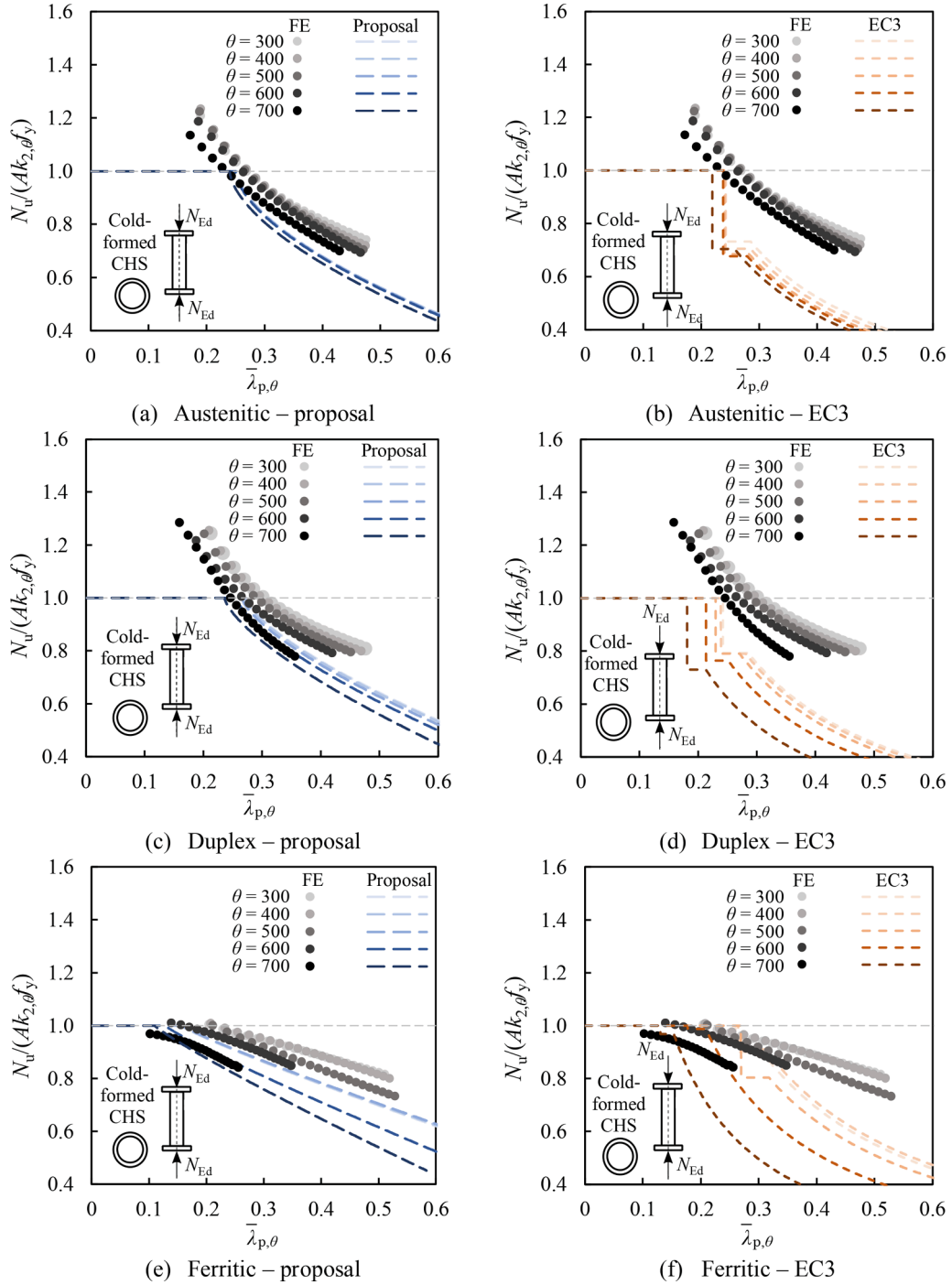
in which W_{pl} is the plastic section modulus and W_{eff} is the effective section modulus given by Eq. (26) where W_{el} is the elastic section modulus.

$$W_{\mathrm{eff}} = \rho W_{\mathrm{el}} \tag{26}$$

In Eq. (26), the local buckling reduction factor ρ is still determined using Eq. (23) for CHS and EHS subjected to bending in fire, but with different values for the auxiliary coefficients β and φ which are given in Table 8 for CHS and EHS in bending. The elevated temperature cross-section slenderness $\bar{\lambda}_{\mathrm{p},\theta}$ and the threshold slenderness $\bar{\lambda}_{\mathrm{p}0,\theta}$ for bending are also calculated through Eqs. (17) and (19) respectively, but using the auxiliary coefficients η provided in Table 8 for the latter. This study recommends the determination of the elastic local buckling stresses σ_{cr} of stainless steel CHS and EHS in bending through the critical buckling stress formula given by Eq. (18) using the equivalent diameters D_{e} provided in Table 1 in line with the approach adopted in [54,55]. The determination of the design cross-section bending moment resistances $M_{\mathrm{fi,t,Rd}}$ of CHS and EHS for temperature θ at time t is also shown in Fig. 8 (b) and Table 9.

4.4. Cross-section resistances of CHS and EHS under combined axial compression and bending in fire

In the case of stainless steel CHS and EHS subjected to combined axial compression and bending in fire, the adoption of a linear interaction relationship between the cross-section axial compression resistances $N_{\mathrm{fi,t,Rd}}$ and bending moment resistances $M_{\mathrm{fi,t,Rd}}$ is recommended for the assessment of the cross-section resistances, in accordance with the proposals made for flat sections in [10]. Thus, the cross-section strength can be assessed as given by Eq. (27).

(a) Austenitic – proposal

(b) Austenitic – EC3

(c) Duplex – proposal

(d) Duplex – EC3
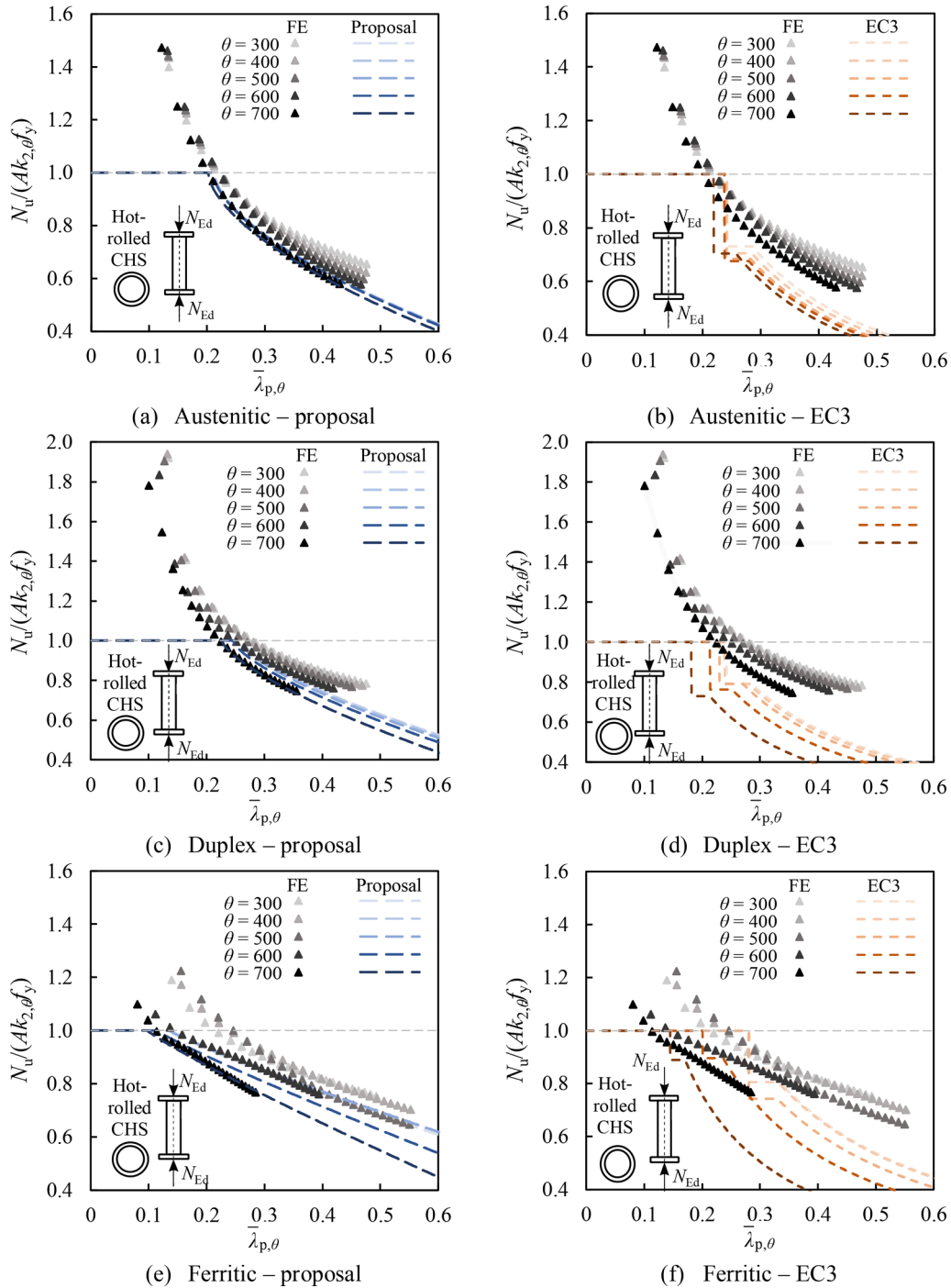
(e) Ferritic – proposal

(f) Ferritic – EC3

Fig. 9. Comparisons of the ultimate resistance predictions obtained using the proposed design method $N_{u,prop}$ and the provisions of EN 1993-1-2 $N_{u,EC3}$, against the benchmark FE predictions $N_{u,FE}$ for cold-formed stainless steel CHS under pure compression at elevated temperatures.

$$\frac{N_{Ed}}{N_{fi,t,Rd}} + \frac{M_{Ed}}{M_{fi,t,Rd}} \leqslant 1.0 \qquad (27)$$

In the proposed fire design approach herein, (i) first, the cross-section axial compression resistances $N_{fi,t,Rd}$ and bending moment resistances $M_{fi,t,Rd}$ of CHS and EHS for temperature θ at time t are calculated independently as described in Section 4.2 and 4.3 and (ii) then, the linear interaction equation given by Eq. (27) is utilised to assess the cross-section resistances of CHS and EHS subjected to combined axial compression and bending in fire. As shown in Fig. 8 (c), if the cross-section is classified as non-slender for both pure compression and pure

bending, the use of the full cross-section area A and the plastic section modulus W_{pl} is recommended for the determination of the cross-section axial compression $N_{fi,t,Rd}$ and bending moment resistances $M_{fi,t,Rd}$ (i.e., $N_{fi,t,Rd} = Ak_{2,\theta}f_y$, $M_{fi,t,Rd} = W_{pl}k_{2,\theta}f_y$). On the other hand, the use of the effective cross-section area A_{eff} and the plastic section modulus W_{pl} is recommended for the determination of the cross-sectional axial force $N_{fi,t,Rd}$ and bending moment resistances $M_{fi,t,Rd}$, when the cross-section is classified as slender under pure axial compression but non-slender under pure bending (i.e., $N_{fi,t,Rd} = A_{eff}k_{2,\theta}f_y$, $M_{fi,t,Rd} = W_{pl}k_{2,\theta}f_y$). Of course, the use of the effective cross-section area A_{eff} and effective section modulus W_{eff} is recommended for the determination $N_{fi,t,Rd}$ and $M_{fi,t,Rd}$, if the

Fig. 10. Comparisons of the ultimate resistance predictions obtained using the proposed design method $N_{u,prop}$ and the provisions of EN 1993-1-2 $N_{u,EC3}$, against the benchmark FE results $N_{u,FE}$ for hot-rolled stainless steel CHS under compression at elevated temperatures at elevated temperatures.

cross-section is classified as slender under both pure axial compression and pure bending cases (i.e., $N_{fi,t,Rd} = A_{eff}k_{2,\theta}f_y$, $M_{fi,t,Rd} = W_{eff}k_{2,\theta}f_y$).

4.5. Cross-section resistances of CHS and EHS under combined bending and shear in fire

To take into consideration the adverse effects of high shear forces on the cross-section resistances of CHS and EHS at elevated temperatures, this study recommends the adoption of an approach in line with that given in the room temperature structural steel design standard EN 1993-1-1 [4] described in Section 3.2. Thus, the reduced cross-section

resistances of CHS and EHS with $V_{Ed} > 0.5V_{fi,t,Rd}$ should be determined through the reduced elevated temperature material strengths at 2% total strain $f_{2,\theta,r}$ which is calculated by Eq. (28).

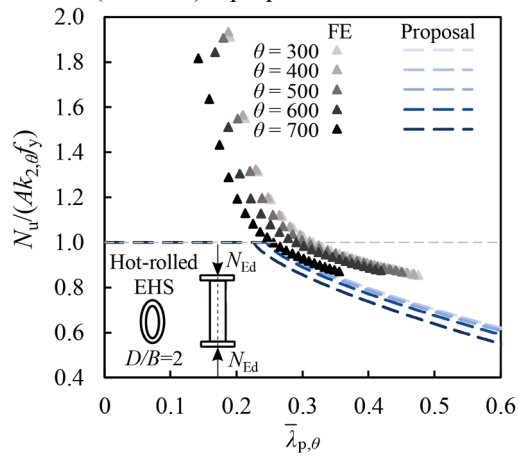$$f_{2,\theta,r} = (1 - \rho_v)k_{2,\theta}f_y \tag{28}$$

In Eq. (28), ρ_v is a reduction factor for the consideration of high shear forces, which should be determined by Eqs. (29) and (30) in line with EN 1993-1-1 [4]. For the determination of the shear areas A_v, the use of the formula provided in EN 1993-1-1 [4] for CHS as given by Eq. (31) and the formulae provided in [49] for EHS as given by Eq. (32) is
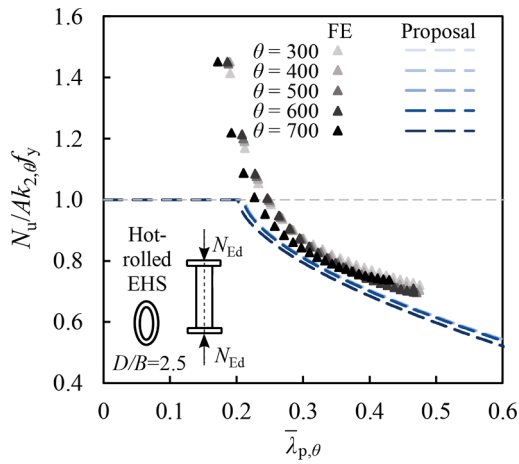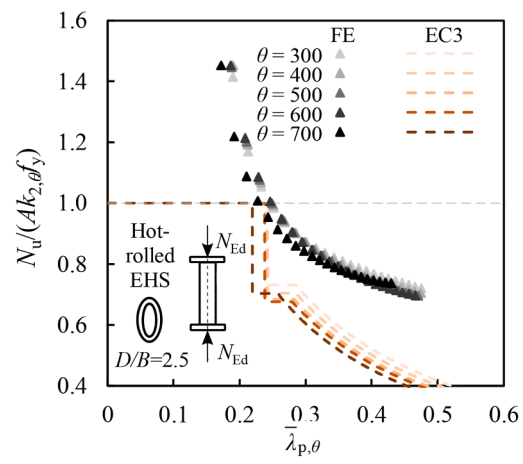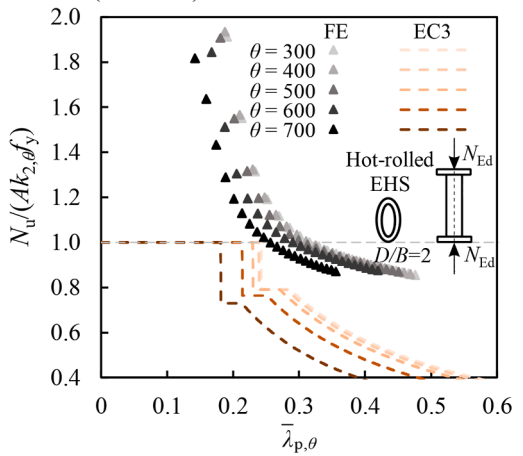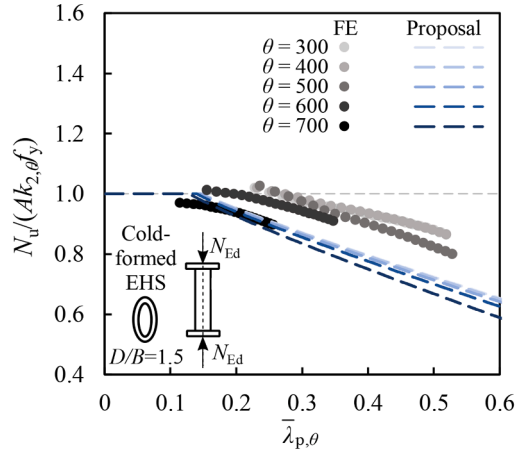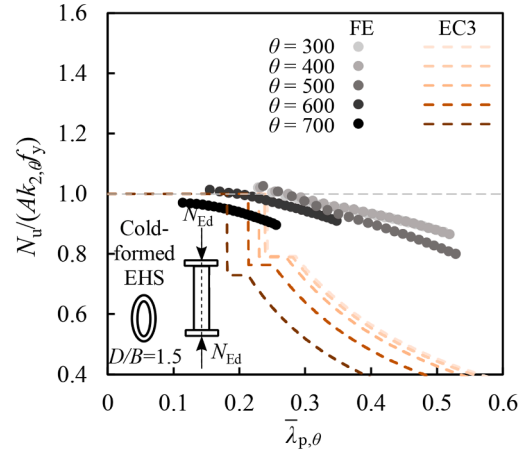
Fig. 11. Comparisons of the ultimate resistance predictions obtained using the proposed design method $N_{u,prop}$ and the provisions of EN 1993-1-2 $N_{u,EC3}$, against the benchmark FE results $N_{u,FE}$ for studied examples of stainless steel EHS under compression at elevated temperatures.
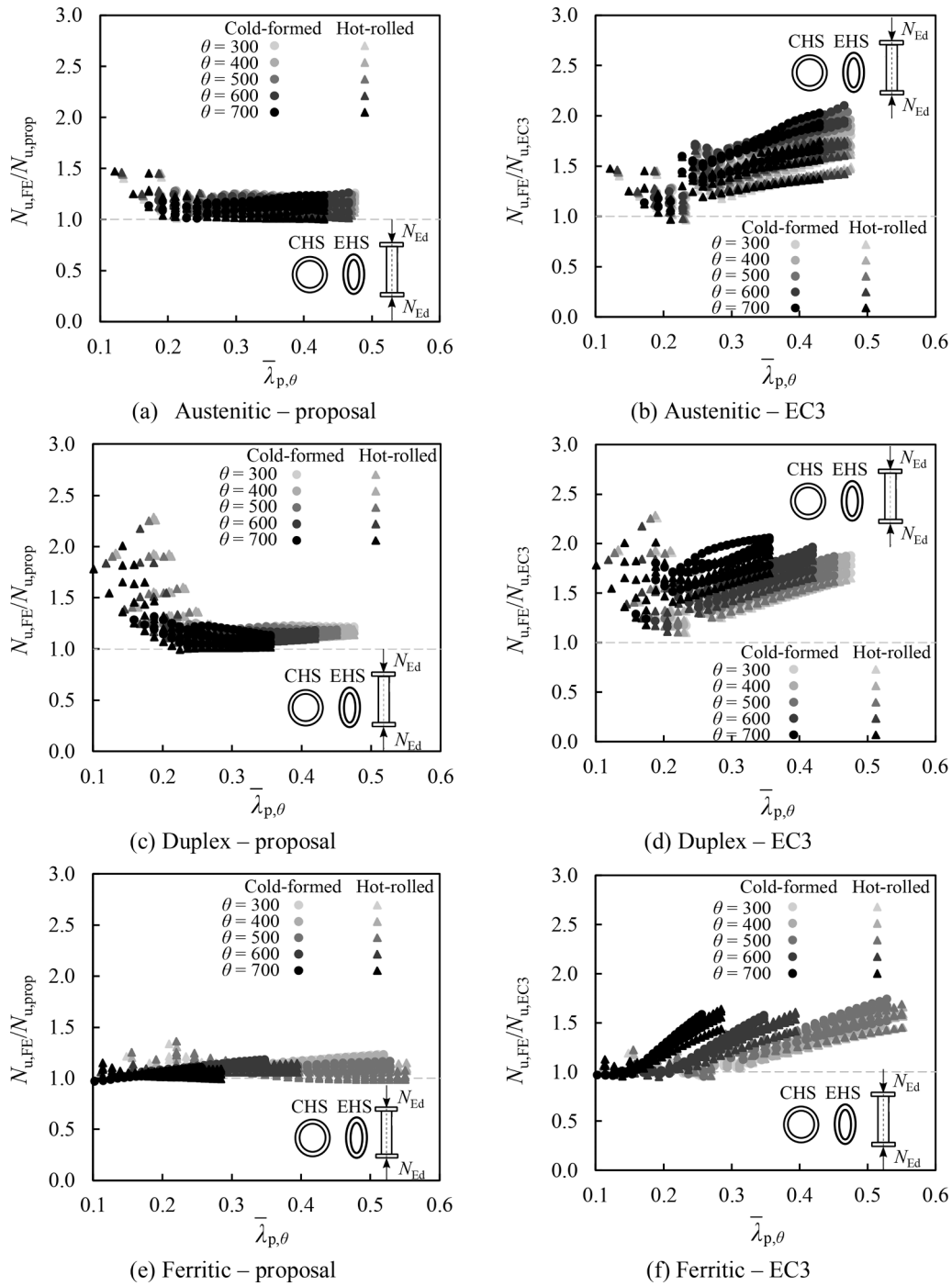
Fig. 12. Assessment of the accuracy of the ultimate cross-section resistance predictions obtained through the proposed design method $N_{\text{u,prop}}$ and the provisions given in EN 1993-1-2 $N_{\text{u,EC3}}$ against those from FE modelling $N_{\text{u,FE}}$ for cold-formed and hot-rolled CHS and EHS under compression at elevated temperatures.

recommended in the implementation of the proposed fire design approach to CHS and EHS subjected to high shear forces in fire.

$$\rho_{\text{v}} = \left(2V_{\text{Ed}}/V_{\text{fi,t,Rd}} - 1\right)^2 \text{ for } V_{\text{Ed}}/V_{\text{fi,t,Rd}} > 0.5 \tag{29}$$

$$V_{\text{fi,t,Rd}} = A_{\text{v}}k_{2,\theta}f_{\text{y}} \tag{30}$$

$$A_{\text{v}} = 2A/\pi \text{ for CHS} \tag{31}$$

$$A_{\text{v}} = \begin{cases} 2t(D - t) \text{ for EHS under major axis bending (load parallel to depth)} \\ 2t(B - t) \text{ for EHS under minor axis bending (load parallel to width)} \end{cases} \tag{32}$$

The proposed approach for the consideration of high shear effects in fire for CHS and EHS is also graphically illustrated in Fig. 8 (d), in which the shear-reduced bending capacity is calculated using the factor $(1-\rho_{\text{v}})$ multiplied by the pure bending capacity at temperature θ. Similarly, the reduced axial compression resistances can also be calculated adopting the same approach if CHS and EHS are subjected to combined axial compression and bending as well as high shear forces.
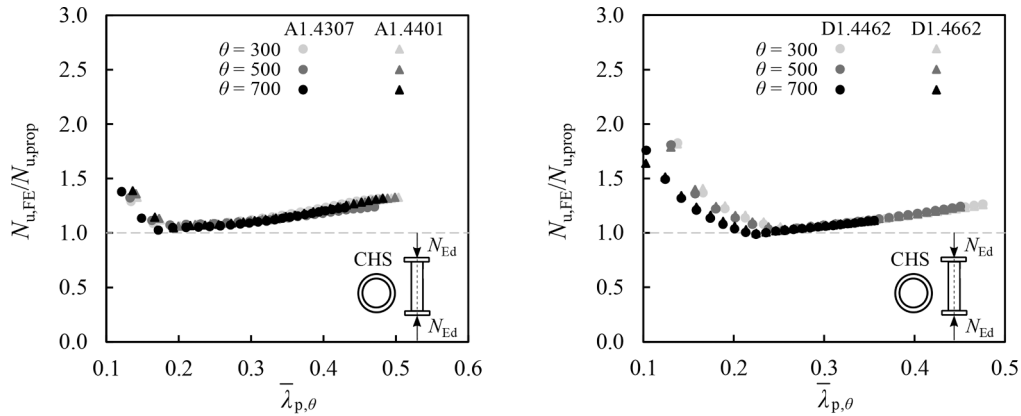
5. Assessment of proposed design methods

In this section, the accuracy of the proposed new fire design rules for CHS and EHS is assessed against the benchmark structural performance

Table 10

Summary of the mean, CoV, maximum and minimum values of the ratios of the resistance predictions obtained from FE modelling $N_{u,FE}$ to those determined using new proposal $N_{u,prop}$ and the provisions of EN 1993-1-2 [3] $N_{u,EC3}$ for all the studied cold-formed and hot-rolled stainless steel CHS and EHS under pure axial compression at elevated temperatures.

Type	Grade	No.	$N_{u,FE}/N_{u,prop}$				$N_{u,FE}/N_{u,EC3}$			
			Mean	CoV	Max	Min	Mean	CoV	Max	Min
Cold-formed	A	395	1.17	0.038	1.28	1.01	1.66	0.119	2.10	1.05
	D	355	1.15	0.043	1.31	1.03	1.66	0.106	2.06	1.16
	F	400	1.11	0.047	1.23	0.97	1.31	0.151	1.74	0.95
Hot-rolled	A	450	1.12	0.067	1.47	1.00	1.43	0.121	1.75	0.96
	D	450	1.19	0.168	2.29	0.99	1.59	0.119	2.29	1.10
	F	450	1.09	0.049	1.36	0.98	1.30	0.139	1.69	0.95

(a) Hot-rolled austenitic 1.4307 and 1.4401

(b) Cold-formed duplex 1.4462 and 1.4662
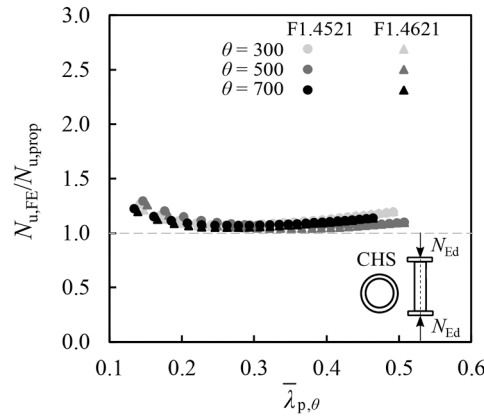
(c) Cold-formed ferritic 1.4521 and 1.4621

Fig. 13. Assessment of the accuracy of the ultimate cross-section resistance predictions obtained through the proposed design method $N_{u,prop}$ against those from FE modelling $N_{u,FE}$ for (a) hot-rolled grade 1.4307 and 1.4401 austenitic stainless steel, (b) cold-formed grade 1.4462 and 1.4662 stainless steel and (c) cold-formed grade 1.4521 and 1.4621 ferritic stainless steel CHS under compression at elevated temperatures; the nominal material properties provided in [5,30] are adopted.

Table 11

Reliability assessment of the proposed design method and the provisions of EN 1993-1-2 [3] for all the studied cold-formed and hot-rolled stainless steel CHS and EHS under pure axial compression at elevated temperatures.

Type	Grade	Proposal			EN 1993-1-2		
		Criterion 1 (%)	Criterion 2 (%)	Criterion 3 (%)	Criterion 1 (%)	Criterion 2 (%)	Criterion 3 (%)
Cold-formed	A	0.00	0.00	−14.77	0.00	0.00	−38.78
	D	0.00	0.00	−12.93	0.00	0.00	−39.04
	F	0.00	1.50	−9.92	0.00	6.50	−21.56
Hot-rolled	A	0.00	0.00	−10.01	0.00	1.11	−29.04
	D	0.00	0.22	−14.34	0.00	0.00	−36.15
	F	0.00	4.00	−8.03	0.00	3.33	−21.71
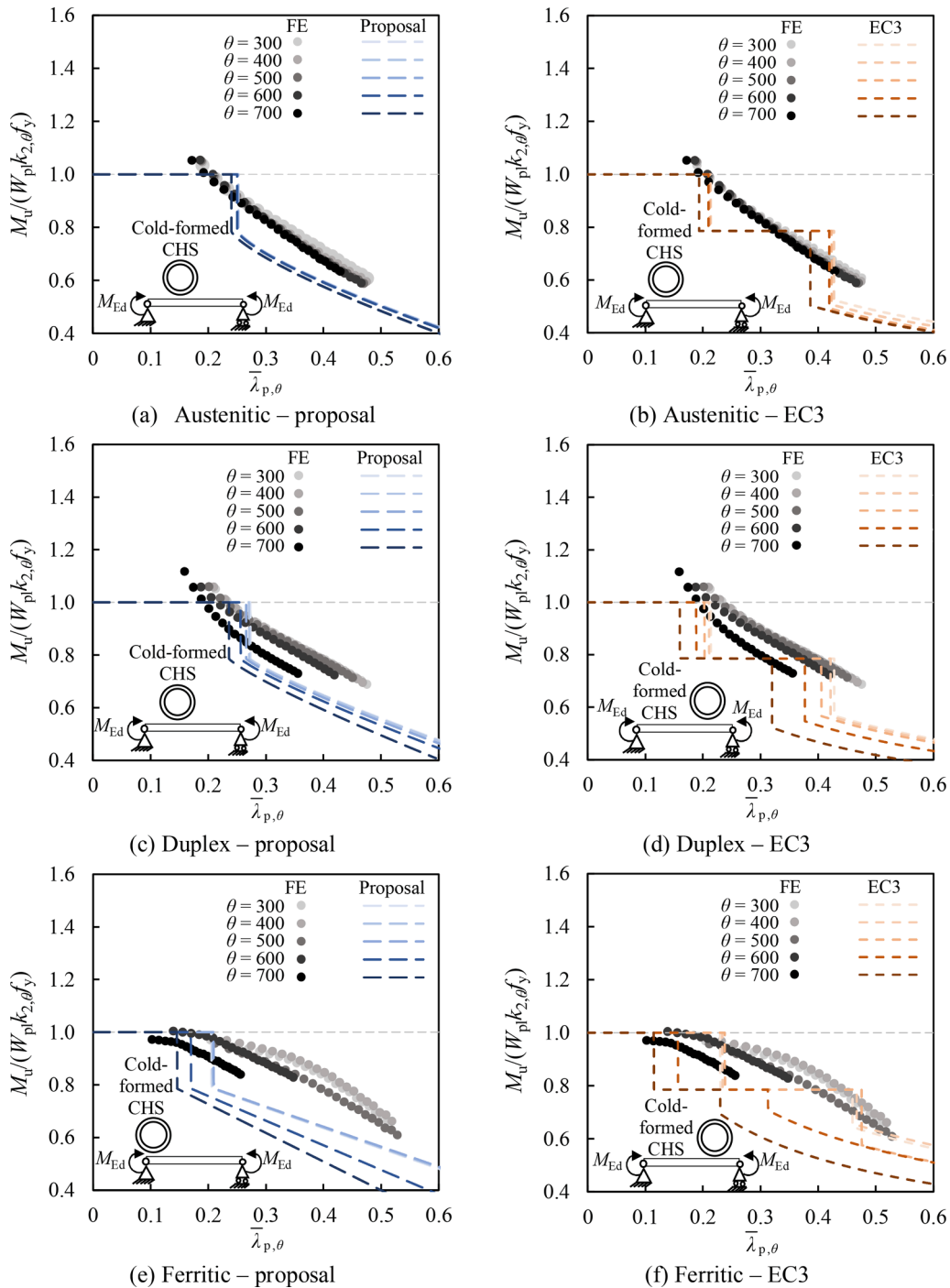
Fig. 14. Comparisons of the ultimate resistance predictions obtained using the proposed design method $M_{u,prop}$ and the provisions in prEN 1993-1-2 $M_{u,EC3}$, against the benchmark FE results $M_{u,FE}$ for cold-formed stainless steel CHS under bending at elevated temperatures.

data obtained from GMNIA, considering a broad range of parameters from the comprehensive parametric studies performed in this paper as set out in Section 2.3. The accuracy of the proposed design rules is also compared against that of the design provisions of EN 1993-1-2 [3] for CHS and EHS in fire.

5.1. Pure axial compression

5.1.1. Accuracy assessment

Figs. 9 and 10 show the comparison of the ultimate resistance predictions obtained using the proposed design method provided in Section 4.1 $N_{u,prop}$ and EN 1993-1-2 [3] (see Section 3.2) $N_{u,EC3}$ against the

benchmark GMNIA ultimate resistances $N_{u,FE}$ for cold-formed and hot-rolled stainless steel CHS under pure axial compression in fire, respectively. As can be seen from the figures, EN 1993-1-2 [3] generally significantly underestimates the ultimate axial compression resistances of CHS and EHS in fire. Due to the transition from the use of the elevated temperature material strengths at 2% total strain $f_{2,\theta} = k_{2,\theta}f_y$ to the use of the elevated temperature 0.2% proof strengths $f_{p0.2,\theta} = k_{p0.2,\theta}f_y$ as the reference material strengths, there are abrupt steps in the cross-section resistances determined through EN 1993-1-2 [3] at the transitions from Class 3 to 4 cross-sections. On the other hand, as can be seen in Figs. 9 and 10, the consistent use of the elevated temperature material strengths at 2% total strain $f_{2,\theta} = k_{2,\theta}f_y$ as the reference material
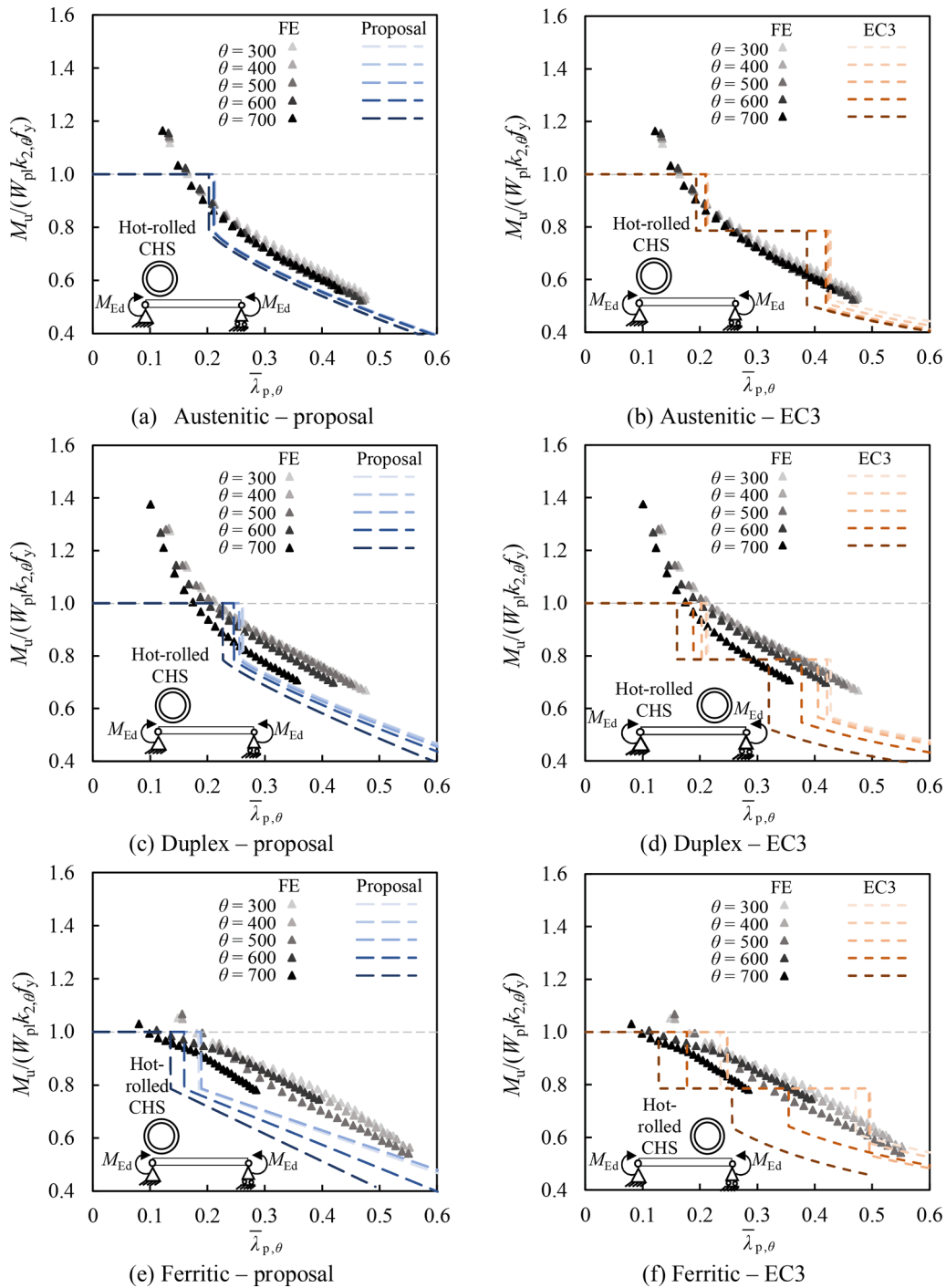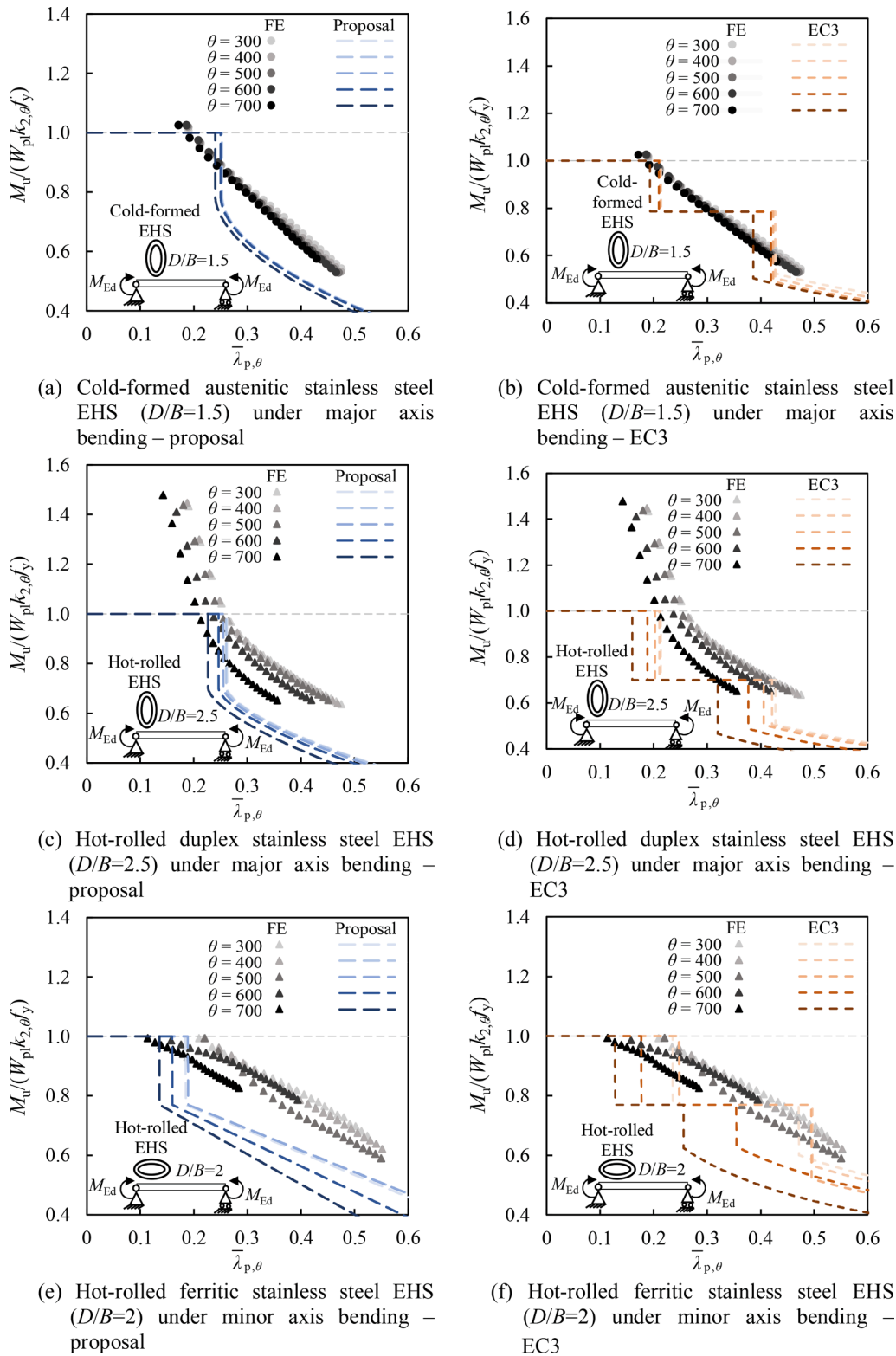
Fig. 15. Comparisons of the ultimate resistance predictions obtained using the proposed design method $M_{\mathrm{u,prop}}$ and the provisions in EN 1993-1-2 $M_{\mathrm{u,EC3}}$, against the benchmark FE results $M_{\mathrm{u,FE}}$ for hot-rolled stainless steel CHS under bending at elevated temperatures.

strengths for the determination of the axial compression resistances for all cross-section classes results in continuous capacity predictions changing with the elevated temperature cross-section slenderness $\bar{\lambda}_{\mathrm{p,\theta}}$ for the proposed design method in this study. Employing (i) the elevated temperature cross-section slenderness $\bar{\lambda}_{\mathrm{p,\theta}}$ and (ii) the recommended β and φ auxiliary coefficients calibrated against the benchmark FE data in the determination of the local buckling reduction factors ρ, the proposed design method provides considerably more accurate ultimate strength predictions for cold-formed and hot-rolled stainless steel CHS subjected to axial compression at different elevated temperature levels relative to EN 1993-1-2 [3] as shown in Figs. 9 and 10. The use of the elevated

temperature slenderness $\bar{\lambda}_{\mathrm{p,\theta}}$ in the determination of the local buckling reduction factors ρ enables the consideration of the differential erosion rates of strength and stiffness of stainless steel at elevated temperatures, thereby leading to an accurate assessment of the behaviour of stainless steel CHS and EHS in fire through the proposed design approach.

The accuracy of the proposed design method is also compared against that of EN 1993-1-2 [3] for different cold-formed and hot-rolled stainless steel EHS subjected to axial compression at elevated temperatures in Fig. 11. As can be seen from Fig. 11, the proposed design method also leads to significantly improved level of accuracy for stainless steel EHS under pure axial compression in fire relative to EN 1993-1-2 [3].

(a) Cold-formed austenitic stainless steel EHS (*D/B*=1.5) under major axis bending – proposal

(b) Cold-formed austenitic stainless steel EHS (*D/B*=1.5) under major axis bending – EC3

(c) Hot-rolled duplex stainless steel EHS (*D/B*=2.5) under major axis bending – proposal

(d) Hot-rolled duplex stainless steel EHS (*D/B*=2.5) under major axis bending – EC3

(e) Hot-rolled ferritic stainless steel EHS (*D/B*=2) under minor axis bending – proposal

(f) Hot-rolled ferritic stainless steel EHS (*D/B*=2) under minor axis bending – EC3

Fig. 16. Comparisons of the ultimate resistance predictions obtained using the proposed design method $M_{u,prop}$ and using the provisions in EN 1993-1-2 $M_{u,EC3}$, against the benchmark FE results $M_{u,FE}$ for studied examples of stainless steel EHS under bending at elevated temperatures.

For the sake of simplicity, the use of the same β and φ auxiliary co-efficients is recommended in the determination of the local buckling reduction factors ρ for both cold-formed and hot-rolled stainless steel CHS and EHS at elevated temperatures in this study. This typically results in slightly more conservative ultimate strength predictions for cold-formed stainless steel CHS and EHS in comparison to their hot-rolled

counterparts, though the discrepancies are not significant as shown in Figs. 9 and 10. Note that owing to the development of lower extents of strain hardening as well as the differences in material properties and elevated temperature reduction factors, ferritic stainless steel cross-sections exhibit structural response that is typically different than that of austenitic and duplex stainless steel cross-sections in fire as shown in
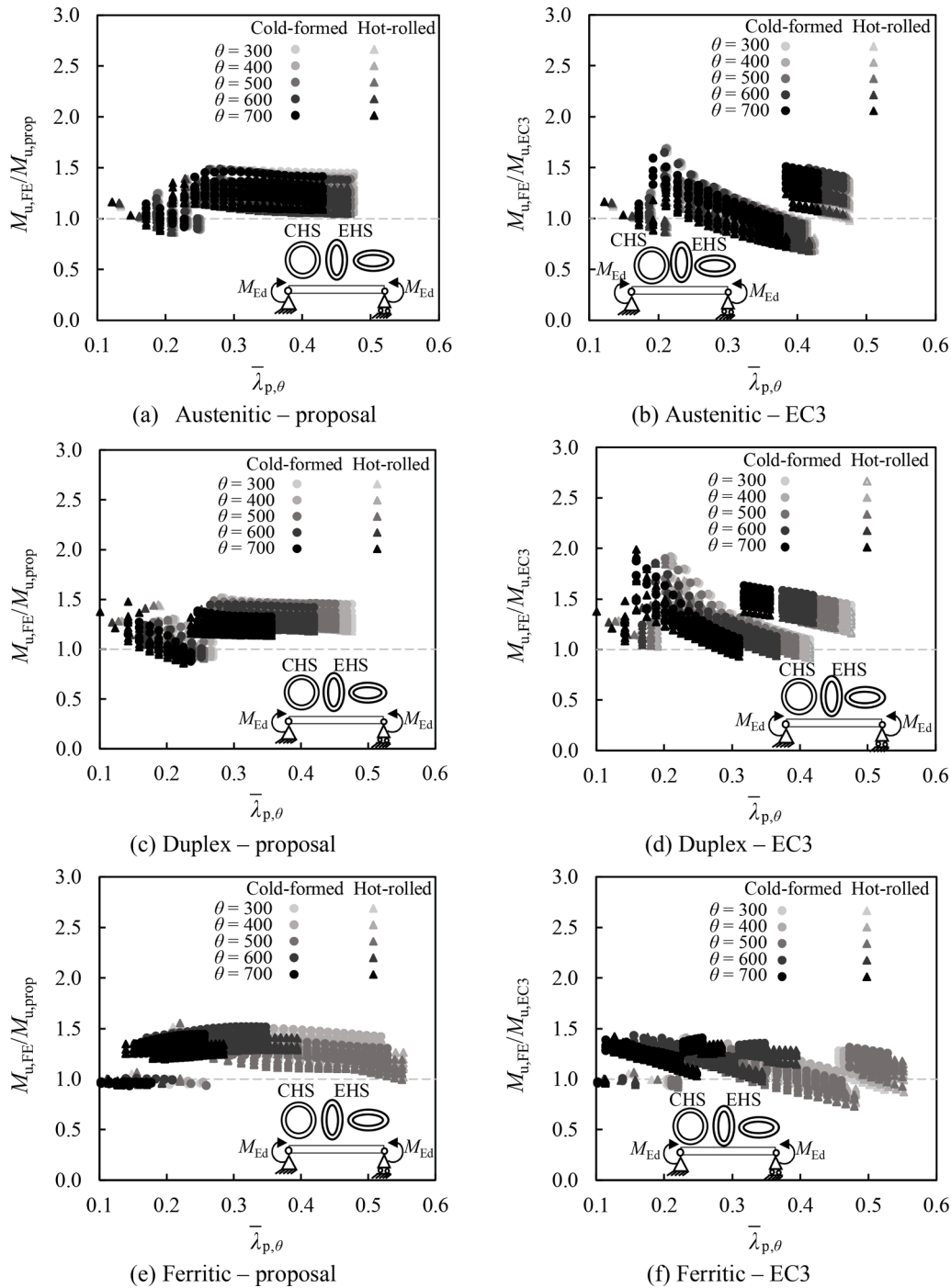
Fig. 17. Assessment of the accuracy of the ultimate cross-section resistance predictions obtained through the proposed design method $M_{u,prop}$ and the provisions given in EN 1993-1-2 $M_{u,EC3}$ against those from FE modelling $M_{u,FE}$ for cold-formed and hot-rolled CHS and EHS under major or minor axis bending at elevated temperatures.

Figs. 9 and 10, which is closer to the behaviour of carbon steel cross-sections at elevated temperatures.

The assessment of the accuracy of the ultimate cross-section resistance predictions obtained through the proposed design method $N_{u,prop}$ and EN 1993-1-2 [3] $N_{u,EC3}$ against those from FE modelling $N_{u,FE}$ is shown in Fig. 12 for all the investigated 2500 cold-formed and hot-rolled CHS and EHS under pure axial compression in fire (see Section 2.3). As can be seen from Fig. 12, relative to the design rules given in EN 1993-1-2 [3], the proposed approach leads to more accurate ultimate resistance predictions with a much lower scatter level for all the considered cold-formed and hot-rolled austenitic, duplex and ferritic CHS and EHS

with a broad range of cross-section properties and subjected to different elevated temperature levels. A statistical appraisal of the accuracy of the proposed design method and EN 1993-1-2 [3] is also provided in Table 10, which summarises the mean, coefficient of variation (CoV), maximum and minimum values of the ratios of the resistance predictions obtained from the FE modelling $N_{u,FE}$ to those determined using the new design method proposed in this paper $N_{u,prop}$ (i,e. $N_{u,FE}/N_{u,prop}$) and EN 1993-1-2 [3] $N_{u,EC3}$ (i.e. $N_{u,FE}/N_{u,EC3}$) for all the studied 2500 cold-formed and hot-rolled stainless steel CHS and EHS under pure axial compression in fire. Note that since the thicknesses of the considered cold-formed CHS and EHS were limited to 6 mm (see Section 2.3), the

Table 12

Summary of mean, CoV, maximum and minimum values of the ratios of the resistance predictions obtained from FE modelling $M_{u,FE}$ to those determined using new proposal $M_{u,prop}$ and the provisions of EN 1993-1-2 [3] $M_{u,EC3}$ for all studied cold-formed and hot-rolled stainless steel CHS and EHS under major or minor axis bending at elevated temperatures.

Type	Grade	No.	$M_{u,FE}/M_{u,prop}$				$M_{u,FE}/M_{u,EC3}$			
			Mean	CoV	Max	Min	Mean	CoV	Max	Min
Cold-formed	A	725	1.24	0.104	1.49	0.89	1.16	0.154	1.69	0.80
	D	680	1.26	0.104	1.51	0.88	1.27	0.141	1.92	0.96
	F	730	1.30	0.100	1.52	0.93	1.18	0.097	1.43	0.85
Hot-rolled	A	780	1.16	0.091	1.40	0.86	0.97	0.153	1.28	0.68
	D	780	1.23	0.104	1.48	0.86	1.24	0.146	1.99	0.92
	F	780	1.23	0.090	1.56	0.94	1.10	0.126	1.42	0.73

Table 13

Reliability assessment of the proposed design method and the provisions in EN 1993-1-2 [3] for all the studied cold-formed and hot-rolled stainless steel CHS and EHS under pure bending at elevated temperatures.

Type	Grade	Proposal			EN 1993-1-2		
		Criterion 1 (%)	Criterion 2 (%)	Criterion 3 (%)	Criterion 1 (%)	Criterion 2 (%)	Criterion 3 (%)
Cold-formed	A	0.00	3.17	−18.36	3.17*	24.14*	−11.41
	D	0.00	7.50	−19.93	0.00	2.06	−20.00
	F	0.00	8.36	−22.44	0.27*	9.04	−14.73
Hot-rolled	A	0.77*	7.18	−13.38	30.64*	57.05*	5.04*
	D	0.26*	8.33	−17.76	0.00	6.03	−17.62
	F	0.00	6.67	−18.30	6.03*	26.67*	−7.27

* Violated criteria.

numbers of the investigated cold-formed cross-sections vary for different stainless steel grades owing to the use of the non-dimensional $(D_e/t)(f_y/235)$ parameter in the determination of the cross-section dimensions (see Table 4) as $(f_y/235)$ changes for different stainless steel grades. As can been seen from Table 10, the mean values of the ratios $N_{u,FE}/N_{u,prop}$ are generally closer to 1.0 with lower CoV values relative to the corresponding mean and COV values of the ratios $N_{u,FE}/N_{u,EC3}$, indicating that the proposed method is able to provide more accurate resistance predictions than EN 1993-1-2 [3] for CHS and EHS subjected to axial compression in fire. Note that the larger CoV value of $N_{u,FE}/N_{u,prop}$ for hot-rolled duplex CHS and EHS was mainly ascribed to the development of considerable extents of strain hardening in stocky sections with low elevated temperature cross-section slendernesses $\bar{\lambda}_{p,\theta}$, as can be seen from Figs. 10-12. Fig. 12 also graphically shows that the design method proposed in this study is able to provide considerably more accurate strength predictions for cold-formed and hot-rolled austenitic, duplex and ferritic CHS and EHS subjected to pure axial compression at elevated temperatures relative to EN 1993-1-2 [3].

It should be noted that the relatively low accuracy of EN 1993-1-2 [3], which will also be shown in the next subsections for the other loading cases, is not surprising since EN 1993-1-2 [3] recommends the use of the room temperature local buckling assessment rules for CHS and EHS provided in EN 1993-1-4 [5] and EN 1993-1-1 [4] with the elevated temperature material properties of stainless steel for the fire design of stainless steel CHS and EHS. Since the elevated temperature material response of stainless steel can be significantly different than its room temperature material response, the behaviour of stainless steel cross-sections in fire may be considerably different than their room temperature behaviour and the development of bespoke fire design rules to consider this significantly different structural response is necessary. The use of specific fire design rules for stainless steel CHS and EHS as those developed in this study leads to considerably more accurate resistance predictions for stainless steel CHS and EHS in fire as illustrated in this paper. Unlike EN 1993-1-2 [3], the cross-section fire design method proposed in this study adopts a new cross-section classification approach in conjunction with new temperature-dependent local buckling reduction factors, thereby providing very accurate cross-section resistance predictions for stainless steel CHS and EHS in fire.

As indicated in Section 2.3, in the parametric studies carried out in this paper, the standardised room temperature material properties recommended in [32] for cold-formed and hot-rolled cross-sections were employed (see Table 2). To consider the influence of different material properties on the structural response, a number of stainless steel CHS stub columns made of different stainless steel grades were also investigated, adopting the nominal material properties provided in the stainless steel design standard EN 1993-1-4 [5] and Steel Construction Institute (SCI) Design Manual for Structural Stainless Steel [30]. The nominal material properties of (i) hot-rolled grade 1.4307 and 1.4401 austenitic stainless steel and cold-formed grade 1.4462 and 1.4662 duplex stainless steel given in EN 1993-1-4 [5] and (ii) the nominal material properties of cold-formed grade 1.4521 and 1.4621 ferritic stainless steel given in the SCI Design Manual for Structural Stainless Steel [30] were considered. To take into account the strength enhancements due to the cold-forming process, the formulae provided in [30] were utilised to calculate the enhanced yield strengths for the considered cold-formed cross-sections and the formulae developed in [23,56] were utilised to calculate the enhanced ultimate strengths, in line with the adoption in [32]. Note that the considered additional stainless steel grades (i.e. 1.4307, 1.4401, 1.4462, 1.4662, 1.4521 and 1.4621) are classified into different material groups for fire design (i.e. I, II and III) in [30]; thus, different elevated temperature material reduction factors given in [30] for the corresponding groups were utilised. Fig. 13 presents the assessment of the ultimate cross-section resistance predictions obtained through the proposed design method $N_{u,prop}$ against those from FE modelling $N_{u,FE}$ for CHS made of the considered additional stainless steel grades in fire; the elevated temperature levels of $\theta = 300\,°C$, $500\,°C$ and $700\,°C$ are considered. It can be seen from Fig. 13 that for the additionally considered stainless steel CHS stub columns made of different austenitic, duplex and ferritic stainless steel grades with the nominal material properties given in [5,30], the proposed design method also provides accurate and safe ultimate resistance predictions at different elevated temperature levels, demonstrating the applicability of the proposed fire design approach to stainless steel cross-sections made of different stainless steel grades with different material properties.
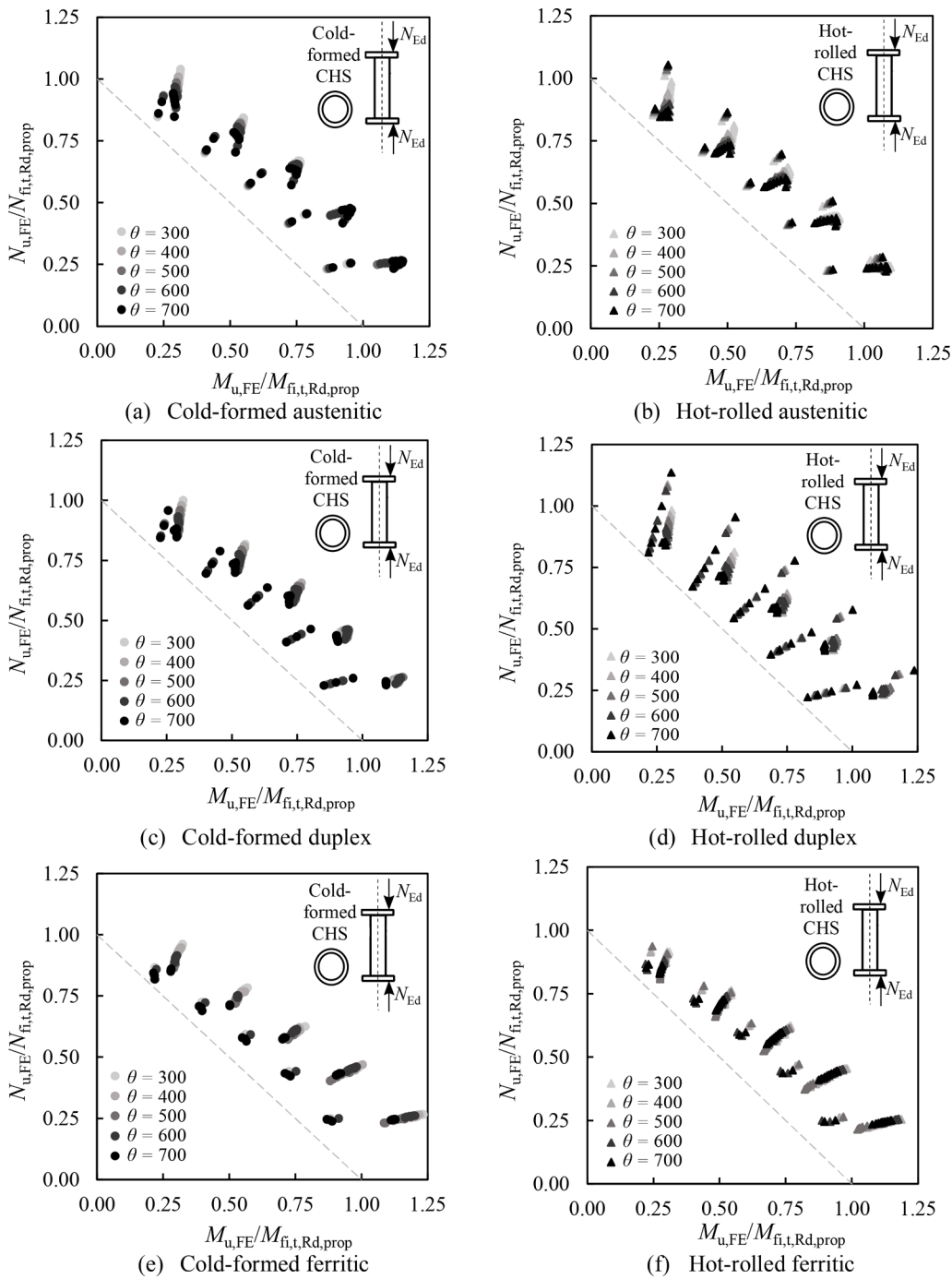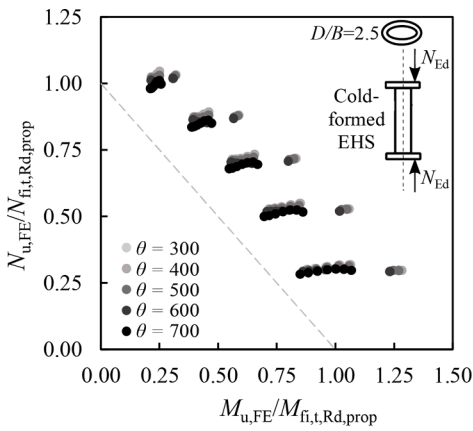
Fig. 18. Interaction relationship between the ultimate compressive resistances obtained from FE modelling $N_{u,FE}$ normalised by the cross-sectional compressive resistances predicted using the proposed design method $N_{fi,t,Rd,prop}$ and the ultimate bending resistances obtained from FE modelling $M_{u,FE}$ normalised by the cross-sectional bending resistances predicted using the proposed design method $M_{fi,t,Rd,prop}$ for studied stainless steel CHS under combined compression and bending at elevated temperatures.

5.1.2. Reliability assessment

The reliability assessment of the proposed design method and EN 1993-1-2 [3] is shown in Table 11 for all the considered 2500 cold-formed and hot-rolled stainless steel CHS and EHS under pure axial compression in fire. In this study, the reliability of the considered fire design methods is assessed through the three reliability criteria put forward by Kruppa [57], which were also used in [58,59,60] and have been approved and adopted by the CEN TC/250 Horizontal Group focusing the development of the European structural steel fire design standard EN 1993-1-2 [3]. The three reliability criteria of Kruppa [57] involve (i) Criterion 1 which requires that none of the strength predictions obtained through a design method should exceed the benchmark FE results by more than 15% (i.e. max [$(N_{u,method} - N_{u,FE})/N_{u,FE}$] ≤ 15%), (ii) Criterion 2 which states that the proportion of the unsafe

strength predictions of a design method should be less than 20% (i.e. num($N_{u,method} > N_{u,FE}$)/num($N_{u,FE}$) ≤ 20%) and (iii) Criterion 3 which requires that the design predictions should be safe-sided on average (i.e. $\bar{X}[(N_{u,method} - N_{u,FE})/N_{u,FE}] < 0\%$). In Table 11, Criterion 1 refers to the percentage of the unsafe strength predictions which exceed the corresponding benchmark FE results by more than 15%, Criterion 2 refers to the percentage of the unsafe strength predictions and Criterion 3 refers to the average percentage difference between the strength predictions and the benchmark FE results. It can be seen from Table 11 that for all the studied cold-formed and hot-rolled stainless steel CHS and EHS stub columns at elevated temperatures, (i) there are no unsafe predictions exceeding the FE results by more than 15% using the proposed design method indicating that the proposed design method satisfies Criterion 1 of Kruppa [57], (ii) the percentage of the unsafe predictions using the
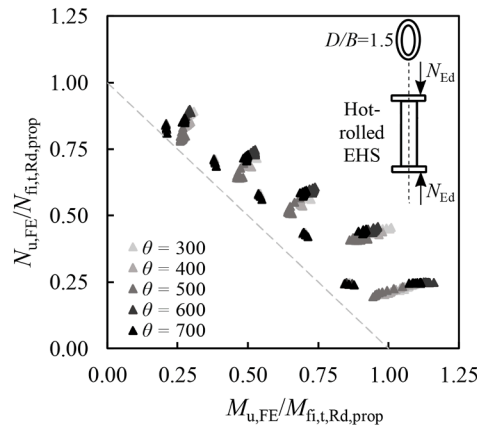
(a) Cold-formed duplex stainless steel EHS (D/B=2.5) under compression and major axis bending
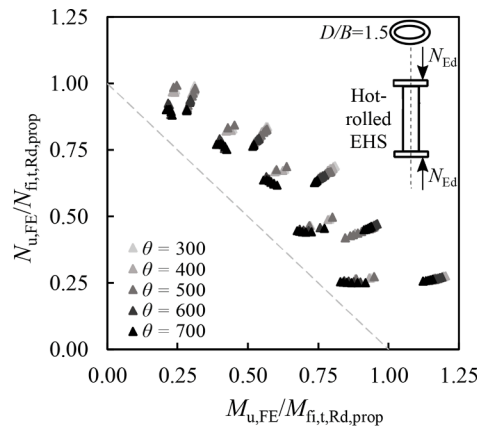
(b) Hot-rolled ferritic stainless steel EHS (D/B=1.5) under compression and major axis bending
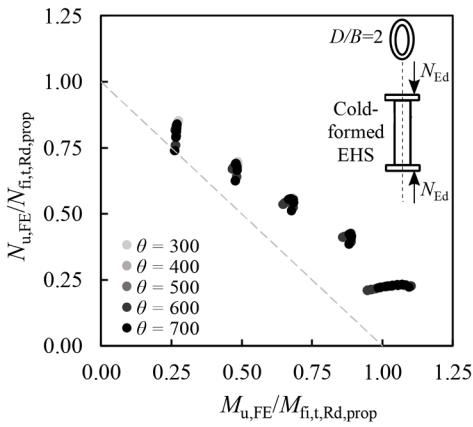
(c) Cold-formed austenitic stainless steel EHS (D/B=2) under compression and minor axis bending

(d) Hot-rolled ferritic stainless steel EHS (D/B=1.5) under compression and minor axis bending

Fig. 19. Interaction relationship between the ultimate compressive resistances obtained from FE modelling $N_{u,FE}$ normalised by the cross-sectional compressive resistances predicted using the proposed design method $N_{fi,t,Rd,prop}$ and the ultimate bending resistances obtained from FE modelling $M_{u,FE}$ normalised by the cross-sectional bending resistances predicted using the proposed design method $M_{fi,t,Rd,prop}$ for studied examples of stainless steel EHS under combined compression and bending at elevated temperatures.

proposed design method (i.e. the percentage of the cases with $N_{u,FE}/N_{u,prop} < 1$) is less than 20% proving that the proposed method satisfies Criterion 2 of [57] and (iii) finally, the average percentage difference between the predictions using the proposed design method and the FE results are negative values which shows that Criterion 3 of [57] is also satisfied by the proposed method. Note that the fire design approach given in EN 1993-1-2 [3] also satisfies all the three reliability criteria of Kruppa [57] as presented in Table 11, though the proposed approach leads to significantly more accurate resistance predictions for CHS and EHS under axial compression in fire as demonstrated in this section.

5.2. Pure bending

5.2.1. Accuracy assessment

In Figs. 14 and 15, the ultimate resistance predictions determined through the proposed design method and EN 1993-1-2 [3] are compared against those obtained from GMNIA for cold-formed and hot-rolled stainless steel CHS under bending in fire. As can be seen from the figures, the proposed design approach leads to an improved level of accuracy relative to EN 1993-1-2 [3] which furnishes quite unsafe predictions for some of the considered cold-formed and hot-rolled stainless steel CHS in bending at elevated temperatures. Note that there are two abrupt steps at the transitions from Class 2 to Class 3 sections and Class 3 to Class 4 sections in the ultimate strength predictions according to EN 1993-1-2 [3] due to (i) the use of the plastic W_{pl} and elastic W_{el} section moduli for the determination of the ultimate resistances of Class 2 and Class 3 sections and (ii) the use of the elevated

temperature material strengths at 2% total strain $f_{2,\theta} = k_{2,\theta}f_y$ and 0.2% proof strengths $f_{p0.2,\theta} = k_{p0.2,\theta}f_y$ for the determination of the ultimate resistances of Class 3 and Class 4 sections, respectively. On the other hand, the proposed method has only one transition owing to the use of the plastic W_{pl} and effective W_{eff} section moduli for non-slender and slender stainless steel CHS and EHS subjected to bending at elevated temperatures. The accuracy of the proposed design method relative to EN 1993-1-2 [3] is also shown in Fig. 16 for a number of different cases of EHS subjected to major or minor axis bending at elevated temperatures. As can be seen from Fig. 16, the proposed design method also leads to improved accuracy for stainless steel EHS subjected to major or minor axis bending in fire relative to EN 1993-1-2 [3].

The ultimate bending resistance predictions obtained through the proposed design method $M_{u,prop}$ and EN 1993-1-2 [3] $M_{u,EC3}$ are also compared against those from GMNIA $M_{u,FE}$ for all the investigated 4475 cold-formed and hot-rolled stainless steel CHS and EHS under major or minor axis bending at elevated temperatures in Fig. 17. It can be seen from the figure that relative to EN 1993-1-2 [3], the proposed approach furnishes significantly more consistent and accurate ultimate bending resistance predictions for the considered 4475 austenitic, duplex and ferritic stainless steel CHS and EHS under uniform bending with a broad range of cross-section properties and subjected to different elevated temperature levels. Fig. 17 also shows that the provisions of EN 1993-1-2 [3] lead to a high number of unsafe resistance predictions for the considered CHS and EHS subjected to bending at elevated temperatures. A statistical assessment of the accuracy of the proposed design method and that of EN 1993-1-2 [3] is also provided in Table 12 for all the
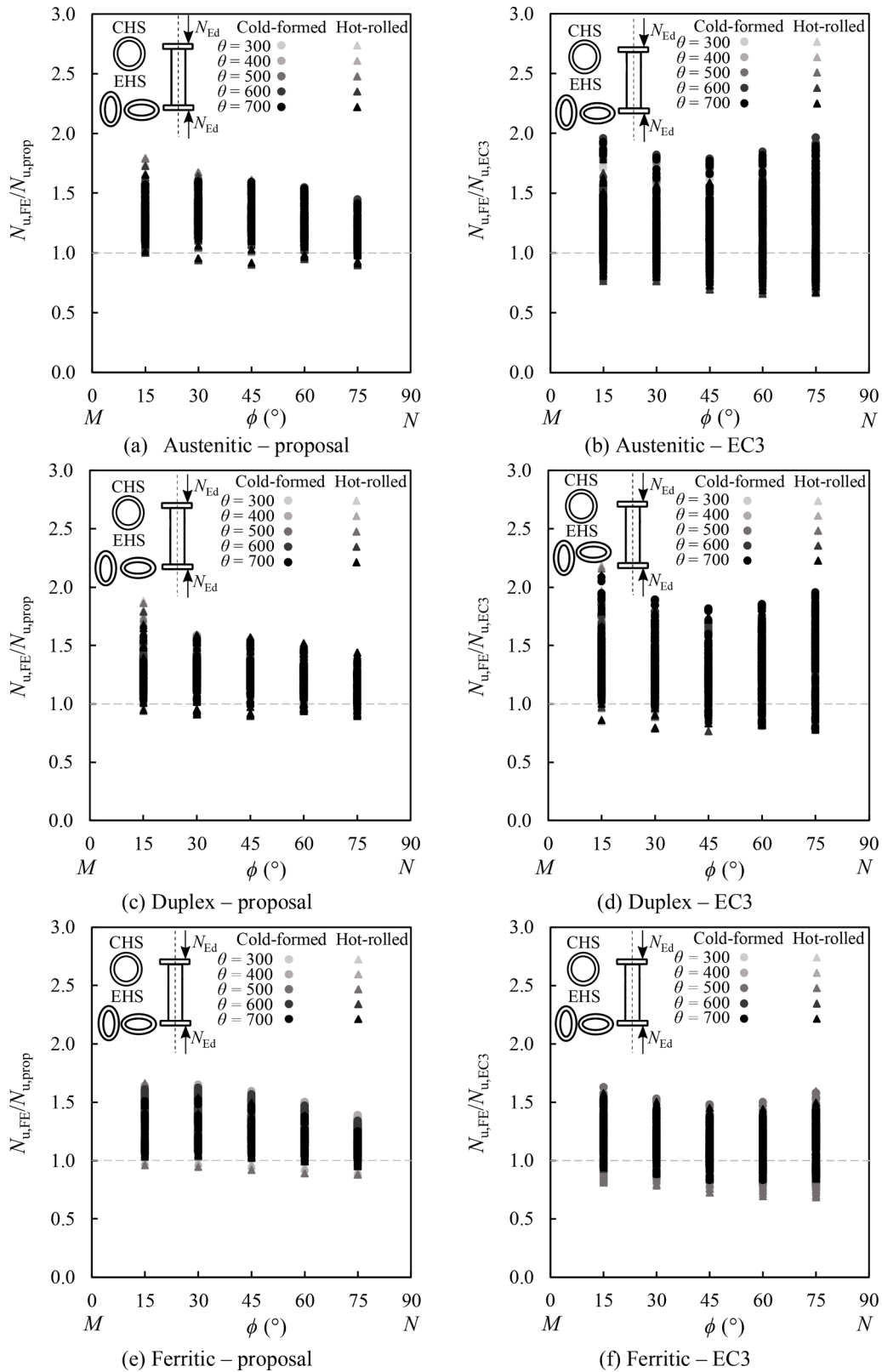
Fig. 20. Assessment of the accuracy of the predicted ultimate axial cross-section resistances determined through the proposed design method $N_{u,prop}$ and the provisions given in EN 1993-1-2 $N_{u,EC3}$ against those from FE modelling $N_{u,FE}$ versus the radial angle ϕ for cold-formed and hot-rolled CHS and EHS under combined compression and bending at elevated temperatures.

Table 14

Summary of mean, CoV, maximum and minimum values of the ratios of the resistance predictions obtained from FE modelling $N_{u,FE}$ to those determined using new proposal $N_{u,prop}$ and the provisions of EN 1993-1-2 [3] $N_{u,EC3}$ for all the studied cold-formed and hot-rolled stainless steel CHS and EHS under combined axial compression and bending at elevated temperatures.

Type	Grade	No.	$N_{u,FE}/N_{u,prop}$				$N_{u,FE}/N_{u,EC3}$			
			Mean	CoV	Max	Min	Mean	CoV	Max	Min
Cold-formed	A	1625	1.29	0.100	1.61	1.00	1.26	0.202	1.96	0.73
	D	1450	1.27	0.086	1.59	0.92	1.32	0.175	2.09	0.78
	F	1675	1.30	0.105	1.65	1.01	1.14	0.137	1.63	0.77
Hot-rolled	A	1950	1.25	0.118	1.80	0.90	1.11	0.198	1.80	0.66
	D	1950	1.25	0.118	1.88	0.89	1.25	0.187	2.18	0.77
	F	1950	1.27	0.112	1.66	0.88	1.10	0.159	1.60	0.68

Table 15

Reliability assessment of the proposed design method and the provisions of EN 1993-1-2 [3] for all the studied cold-formed and hot-rolled stainless steel CHS and EHS under combined axial compression and bending at elevated temperatures.

Type	Grade	Proposal			EN 1993-1-2		
		Criterion 1 (%)	Criterion 2 (%)	Criterion 3 (%)	Criterion 1 (%)	Criterion 2 (%)	Criterion 3 (%)
Cold-formed	A	0.00	0.25	−21.57	4.18*	16.06	−17.53
	D	0.00	0.76	−20.36	2.28*	7.03	−21.79
	F	0.00	0.00	−22.40	2.33*	21.37*	−10.85
Hot-rolled	A	0.00	2.56	−19.10	13.64*	32.87*	−6.76
	D	0.00	5.13	−19.08	3.69*	13.85	−17.07
	F	0.00	1.95	−20.52	7.23*	33.64*	−6.64

* Violated criteria.

studied 4475 cold-formed and hot-rolled stainless steel CHS and EHS subjected to bending in fire. Table 12 shows that the differences between the mean values of the ratios of $M_{u,FE}/M_{u,prop}$ and $M_{u,FE}/M_{u,EC3}$ are not as high as those observed for pure axial compression cases in the previous subsection and the mean values of $M_{u,FE}/M_{u,EC3}$ are generally closer to 1.0. However, this is due to the large proportion of unsafe ultimate strength predictions obtained using EN 1993-1-2 [3] as shown in Table 12 and Fig. 17. Generally, the proposed design method provides accurate but still safe-sided resistance predictions with lower CoV values relative to EN 1993-1-2 [3] as can be seen from Table 12 and Fig. 17, indicating that it leads to a higher level of accuracy, safety and consistency relative to EN 1993-1-2 [3] for the ultimate resistance predictions of stainless steel CHS and EHS under bending in fire.

5.2.2. Reliability assessment

The reliability assessment of the proposed design method and that of EN 1993-1-2 [3] according to the reliability criteria of Kruppa [57] is summarised in Table 13. As can be seen from the table, the proposed design method only very slightly (only by 0.26% and 0.77%) violates the Criterion 1 of Kruppa [57] for hot-rolled austenitic and duplex stainless steel CHS and EHS in bending (as highlighted with '*') which can be deemed to be acceptable and satisfies all the other reliability criteria of [57]. On the other hand, as can be seen in Table 13, EN 1993-1-2 [3] significantly violates the reliability criteria of [57] in a high number of cases with the violation of the all criteria for one group owing to (i) the most unsafe resistance predictions exceeding the benchmark FE results by more than 15% (i.e. the violation of Criterion 1 of [57]), (ii) the percentage of unsafe predictions higher than 20% (i.e. the violation of Criterion 2 of [57]) and (iii) the design predictions located on the unsafe-side on average (i.e. the violation of Criterion 3 of [57]). This proves that unlike EN 1993-1-2 [3], the proposed design method leads to reliable ultimate resistance predictions for cold-formed and hot-rolled austenitic, duplex and ferritic stainless steel CHS and EHS subjected to bending at different elevated temperature levels.

5.3. Combined compression and bending

5.3.1. Accuracy assessment

According to the design method proposed in this study, the ultimate

cross-section resistances of stainless steel CHS and EHS subjected to combined axial compression and bending in fire are determined assuming a linear interaction between the pure axial compression and pure bending resistances through Eq., as shown in Fig. 8 and described in Section 4.3. Fig. 18 presents the ultimate strengths of CHS stub beam-columns subjected to combined axial compression and bending. In Fig. 18, (i) the axial compression resistances obtained from the GMNIA $N_{u,FE}$ are normalised by the cross-section axial compression resistances determined using the proposed design method $N_{fi,t,Rd,prop}$ (i.e. $N_{u,FE}/N_{fi,t,Rd,prop}$) and (ii) the bending moment resistances obtained from the GMNIA $M_{u,FE}$ are normalised by the cross-section bending moment resistances predicted through the proposed design method $M_{fi,t,Rd,prop}$ (i.e. $M_{u,FE}/M_{fi,t,Rd,prop}$). All the studied cold-formed and hot-rolled stainless steel CHS stub beam-columns are taken into consideration and the linear interaction diagrams using the axial compression and bending moment resistances as proposed in this study are also included in Fig. 18. It can be seen from Fig. 18 that the proposed linear interaction equation given by Eq. leads to safe and generally accurate ultimate resistance predictions for stainless steel CHS under combined axial compression and bending in fire when the normalised ultimate resistances from the GMNIA are considered. Similar observations can also be made for stainless steel EHS subjected to combined axial compression and bending at elevated temperatures in Fig. 19, which presents the comparison between the normalised FE results (i.e. $N_{u,FE}/N_{fi,t,Rd,prop}$ versus $M_{u,FE}/M_{fi,t,Rd,prop}$) and the proposed linear interaction approach for different EHS stub beam-columns subjected to combined axial compression and major or minor axis bending at elevated temperatures.

The accuracy of the ultimate axial compression resistances predicted through the proposed design method $N_{u,prop}$ and EN 1993-1-2 $N_{u,EC3}$ against those from the GMNIA $N_{u,FE}$ is assessed in Fig. 20 for all the investigated 10,600 cold-formed and hot-rolled CHS and EHS stub beam-columns subjected to combined axial compression and major or minor axis bending with different radial angles ϕ. As described in Fig. 7, the parameter radial angle ϕ determined using Eq. provides an indication of the intensities of the applied axial compression and bending where $\phi = 0°$ and $\phi = 90°$ correspond to pure bending and pure axial compression, respectively. It can be seen from Fig. 20 that for different axial compression and bending moment intensity levels, the proposed design method leads to more accurate resistance predictions with a
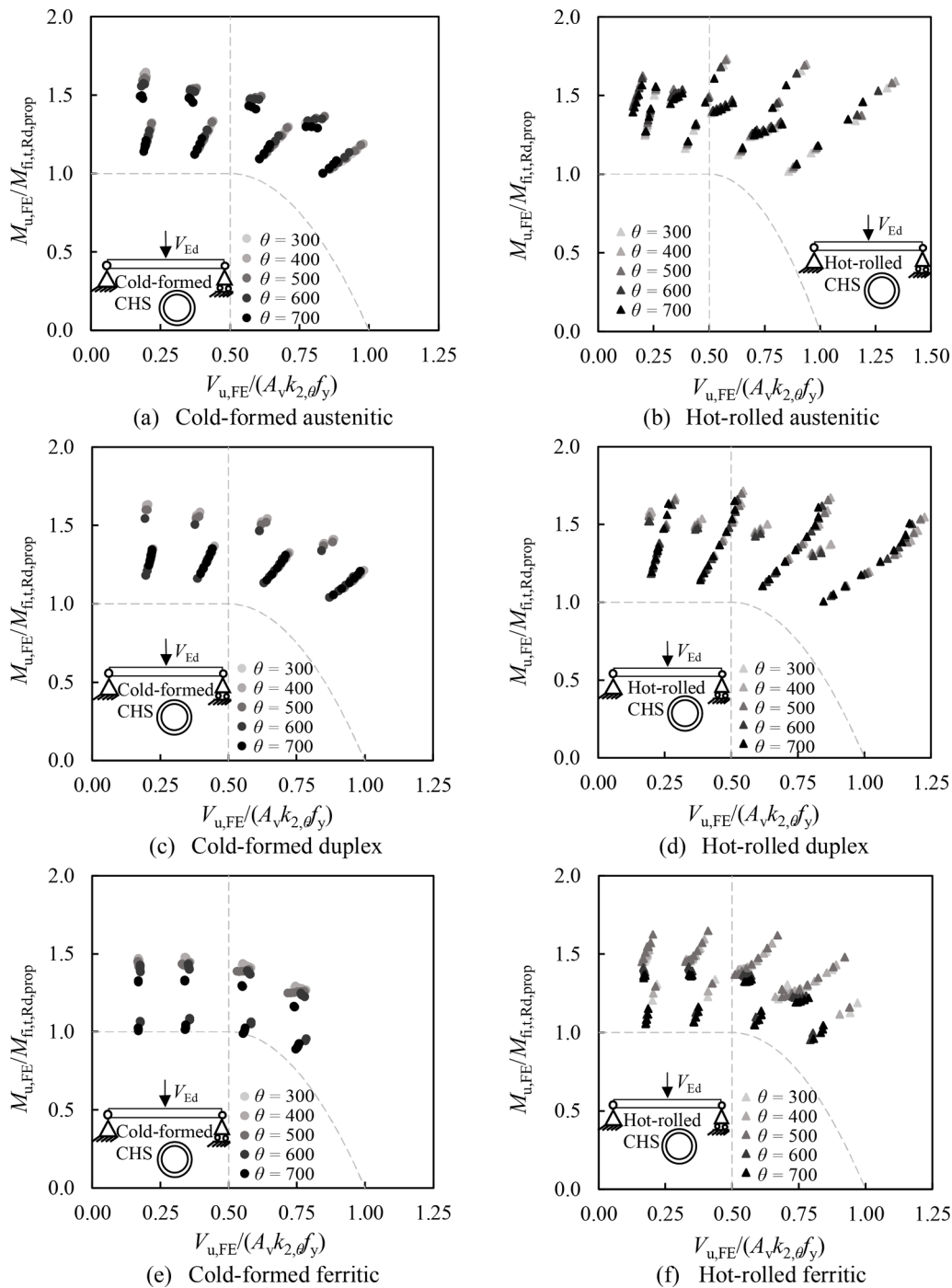
Fig. 21. Interaction relationship between the ultimate shear resistances obtained from FE modelling $V_{u,FE}$ normalised by the plastic cross-section shear resistances $A_v k_{2,\theta} f_y$ and the ultimate bending moment resistances obtained from FE modelling $M_{u,FE}$ normalised by the cross-section bending moment resistances predicted using the proposed design method $M_{fi,t,Rd,prop}$ for studied stainless steel CHS members under 3-point bending at elevated temperatures.
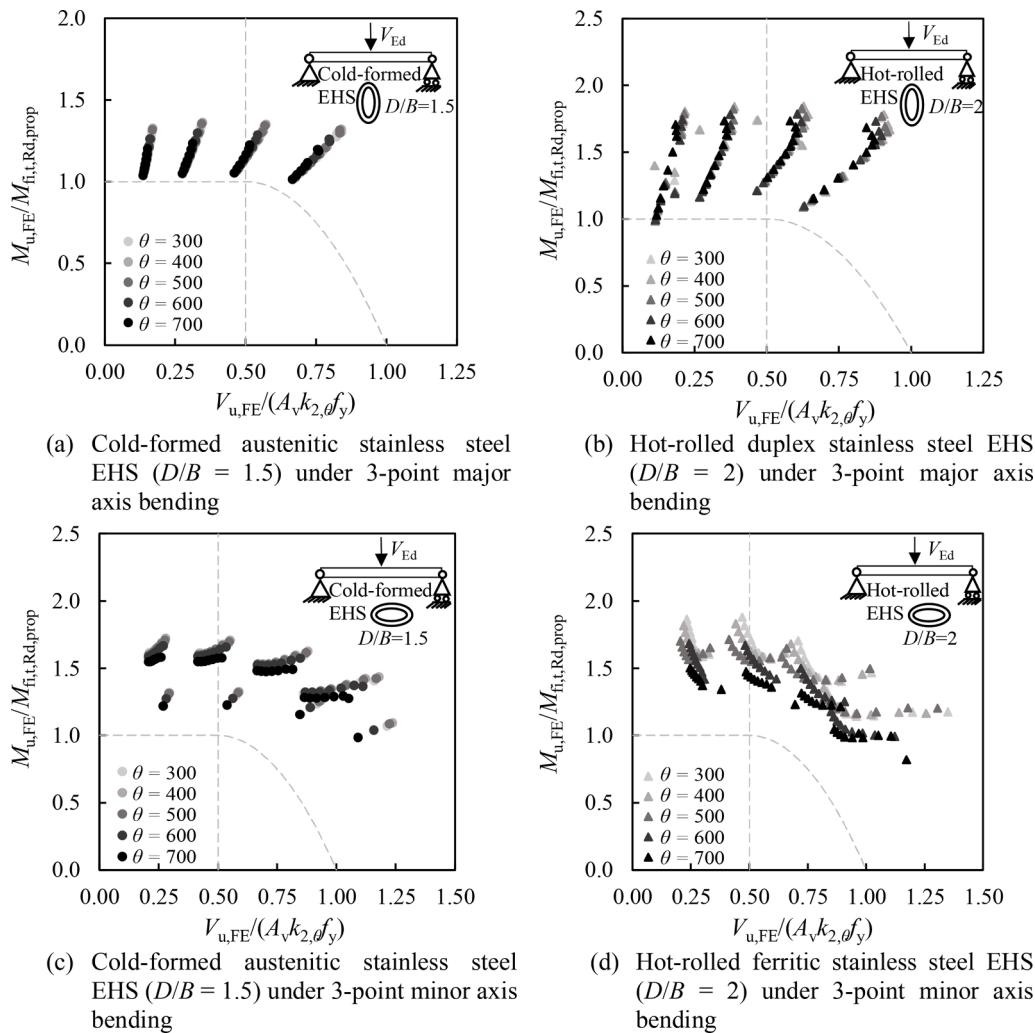
significantly lower level of scatter relative to EN 1993-1-2 [3] for the considered broad range of cold-formed and hot-rolled stainless steel CHS and EHS stub beam-columns in fire. On the other hand, a large proportion of the EN 1993-1-2 [3] ultimate resistance predictions are unsafe as can be seen from Fig. 20.

Table 14 provides a statistical assessment of the accuracy of the proposed design method and EN 1993-1-2 [3], taking into consideration all the studied 10,600 cold-formed and hot-rolled austenitic, duplex and ferritic stainless steel CHS and EHS stub beam-columns subjected to combined axial compression and major or minor axis bending in fire. It can be seen from the table that the proposed design method provides

accurate but still safe-sided resistance predictions with lower CoV values relative to EN 1993-1-2 [3], indicating that it leads to more accurate, safe and consistent ultimate resistance predictions for all the considered high number of cold-formed and hot-rolled stainless steel CHS and EHS subjected to combined axial compression and bending at elevated temperatures.

5.3.2. Reliability assessment

It can be seen from Table 15 that the proposed design method fulfils all the three reliability criteria of Kruppa [57], while EN 1993-1-2 [3] violates the Criterion 1 for all the groups, taking into account the most unsafe

(a) Cold-formed austenitic stainless steel EHS (D/B = 1.5) under 3-point major axis bending

(b) Hot-rolled duplex stainless steel EHS (D/B = 2) under 3-point major axis bending

(c) Cold-formed austenitic stainless steel EHS (D/B = 1.5) under 3-point minor axis bending

(d) Hot-rolled ferritic stainless steel EHS (D/B = 2) under 3-point minor axis bending

Fig. 22. Interaction relationship between the ultimate shear resistances obtained from FE modelling $V_{u,FE}$ normalised by the plastic cross-section shear resistances $A_v k_{2,\theta} f_y$ and the ultimate bending resistance obtained from FE modelling $M_{u,FE}$ normalised by the cross-section bending moment resistances predicted using the proposed design method $M_{fi,t,Rd,prop}$ for studied examples of stainless steel EHS members under 3-point bending at elevated temperatures.

resistance predictions from EN 1993-1-2 [3] exceeding the benchmark FE results by more than 15% in all cases. EN 1993-1-2 [3] also violates Criterion 2 for the considered hot-rolled austenitic and cold-formed and hot-rolled ferritic stainless steel stub beam-columns owing to the percentage of the unsafe predictions being greater than 20%.

5.4. Combined bending and shear

For the case of combined bending and shear in fire, this study recommends that when the applied shear force V_{Ed} exceeds half of the plastic cross-section shear resistance $V_{pl} = A_v k_{2,\theta} f_y$ (i.e. $V_{Ed} > 0.5 A_v k_{2,\theta} f_y$), the cross-section bending moment capacity needs to be reduced considering the high shear effects, as described in Section 4.4. Using the approach put forward in Section 4.4, the normalised bending moment-shear interaction diagrams for the studied stainless steel CHS beams in fire are compared against the ultimate resistances determined through the GMNIA for the CHS beams with varying lengths as shown in Fig. 21, where $V_{u,FE}$ is the ultimate shear resistance determined through the GMNIA. The normalised moment-shear interaction diagrams for the studied examples of stainless steel EHS at elevated temperatures are also presented in Fig. 22. Note that in some cases where large shear deformations occurred and no peak loads were attained, the ultimate resistances were defined considering the applied loads at which the tangent stiffnesses of the load-deformation curves degraded to 1% of the initial stiffness following the approach put

forward in dos Santos et al. [61] and also adopted in [62,63]. It can be seen from Figs. 21 and 22 that the proposed approach for the consideration of bending-shear interaction leads to safe-sided ultimate resistance predictions. It should be noted that due to strain hardening and the effective increase in the elevated temperature strengths under multiaxial stress conditions, some cross-sections continue to resist increasing shear forces after the applied bending moments exceed the plastic cross-section bending moment resistances as can be seen from Figs. 21 and 22, which was also observed in previous research [64].

In Fig. 23, the accuracy of the bending moment resistance predictions of the proposed design method $M_{u,prop}$ against those from FE modelling $M_{u,FE}$ are shown for all the investigated 6920 cold-formed and hot-rolled austenitic, duplex and ferritic stainless steel CHS and EHS members subjected to combined bending and shear at elevated temperatures (see Section 2.3 for all the considered parameters). Fig. 23 shows that the proposed design method leads to safe capacity predictions for CHS and EHS subjected to combined bending and shear in fire, taking into account a very large number of parameters set out in Section 2.3. Since this study adopts a design approach similar to that given in EN 1993-1-2 [3] to consider the combination of bending and shear, the assessment of the calculations with reference to EN 1993-1-2 [3] is not presented. It should be noted that in this study, CHS and EHS susceptible to shear buckling were not taken into account; the shear buckling behaviour and design of CHS and EHS in fire will be extensively investigated in future research.
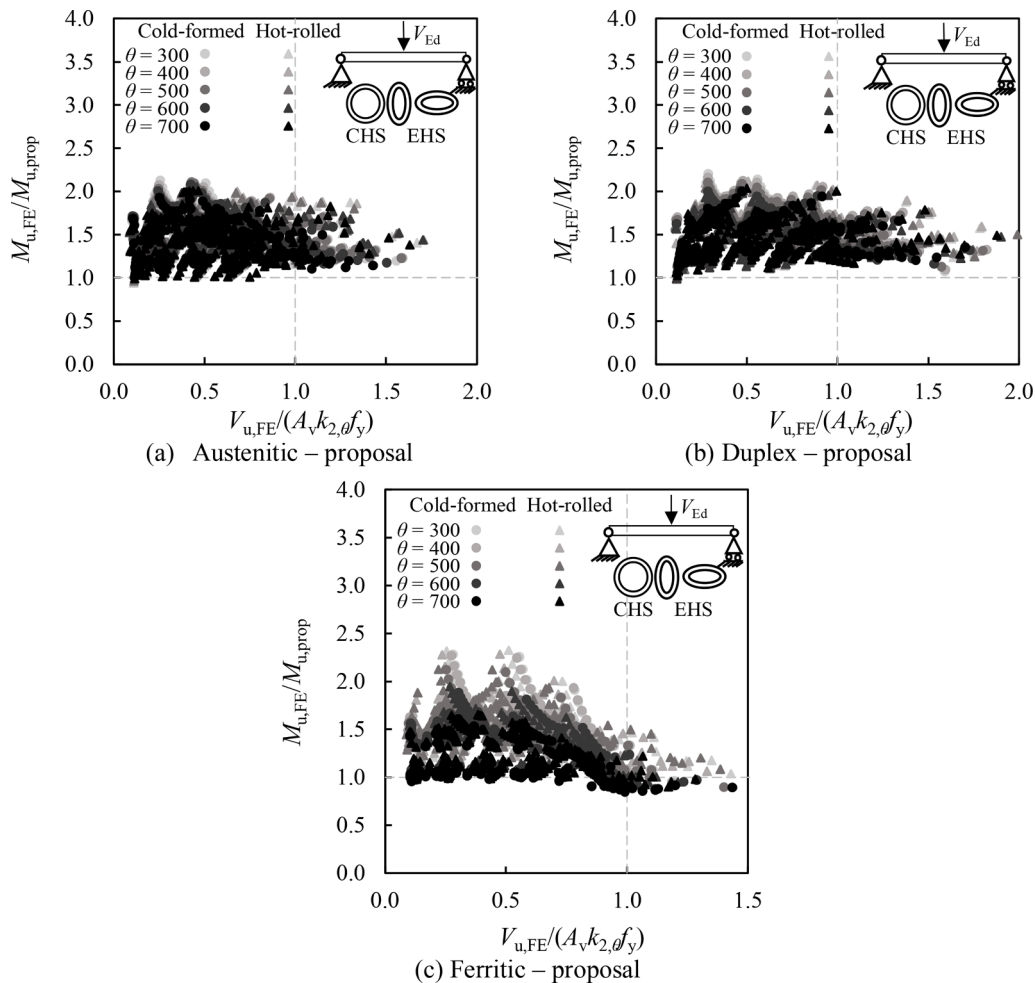
Fig. 23. Assessment of the accuracy of the predicted bending moment resistances through the proposed design method $M_{u,prop}$ against those from FE modelling $M_{u,FE}$ for cold-formed and hot-rolled CHS and EHS under 3-point bending at elevated temperatures.

6. Conclusions

In this paper, the behaviour and design of stainless steel circular hollow sections (CHS) and elliptical hollow sections (EHS) at elevated temperatures have been investigated. Shell FE models of CHS and EHS members were created and validated against experimental results from literature. Following their validation, the FE models were used to carry out numerical parametric studies to generate benchmark structural performance data. Both cold-formed and hot-rolled austenitic, duplex and ferritic stainless steel CHS and EHS were considered; the considered loading conditions comprised (i) pure compression, (ii) pure bending, (iii) combined compression and bending and (iv) combined bending and shear. Various elevated temperature levels and cross-sections slendernesses were taken into consideration. Moreover, different intensities of axial compression, bending moment and shear were accounted for in the combined loading cases. In total, 24,495 CHS and EHS members in fire were taken into account in the parametric studies, considering (i) 2500 stub columns, (ii) 4475 uniform bending cases, (iii) 10,600 stub beam-columns subjected to combined axial compression and bending and (iv) 6920 three-point bending cases where combined shear and bending was applied to the investigated members. Calibrated against the benchmark FE results, new cross-section design methods for stainless steel CHS and EHS subjected to different loading conditions in fire were developed in this study. The accuracy of the proposed design methods was assessed for all the considered cases and also compared against that of the European structural steel fire design standard EN 1993-1-2 [3]. It was observed that relative to EN 1993-1-2 [3], the proposed fire design methods generally

lead to more accurate and safe-sided cross-section resistance predictions with lower levels of scatter for stainless steeel CHS and EHS in fire. The reliability of the proposed design methods was also assessed using the three fire reliability criteria put forward by Kruppa [57] for all the considered cases. The proposed design methods only very slightly (only by 0.26% and 0.77%) violated the Criterion 1 of Kruppa [57] for very few cases, which can be deemed to be acceptable, and satisfied all the other reliability criteria of [57] for all the considered cases. On the other hand, it was shown that EN 1993-1-2 [3] significantly violated the reliability criteria of [57] in a high number of cases, proving that the proposed design methods provide more reliable ultimate resistance predictions for CHS and EHS in fire relative to EN 1993-1-2 [3]. In this study, the cross-section behaviour and design of stainless steel CHS and EHS in fire were explored. Future research will focus on (i) the fire design of other stainless steel cross-sections such as rectangular and square hollow sections as well as (ii) the flexural buckling behaviour and design of stainless steel members with CHS and EHS at elevated temperatures.

CRediT authorship contribution statement

Chunyan Quan: Methodology, Software, Validation, Formal analysis, Investigation, Data curation, Writing – original draft, Visualization. **Merih Kucukler:** Conceptualization, Investigation, Writing – original draft, Writing – review & editing, Supervision, Project administration, Funding acquisition.

Declaration of Competing Interest

The authors declare that they have no known competing financial interests or personal relationships that could have appeared to influence the work reported in this paper.

Acknowledgements

References

[1] Gardner L. Stainless steel structures in fire. Proc Inst Civ Eng Struct Build 2007; 160:129–38.

[2] Arrais F, Lopes N, Vila Real P. Design of stainless steel elliptical hollow sections columns in case of fire: parametric study. In: Proceedings of the Eurosteel conference 2021, Sheffield, UK, CE/Papers, vol. 4; 2021. p. 1437–46.

[3] EN 1993-1-2. Eurocode 3: Design of Steel Structures-Part 1-2: General Rules – Structural Fire Design, European Committee for Standardization, Brussels; 2005.

[4] EN 1993-1-1. Eurocode 3: Design of steel structures - Part 1-1: General rules and rules for buildings. European Committee for Standardization, Brussels; 2005.

[5] EN 1993-1-4:2006 + A1: 2015. Eurocode 3: Design of steel structures - Part 1-4: General rules - Supplementary rules for stainless steels. Brussels, 2015.

[6] Ranby A. Structural fire design of thin walled steel sections. J Constr Steel Res 1998;1(46):303–14.

[7] Kucukler M. Local stability of normal and high strength steel plates at elevated temperatures. Eng Struct 2021;243:112528.

[8] Knobloch M, Fontana M. Strain-based approach to local buckling of steel sections subjected to fire. J Constr Steel Res 2006;62(1–2):44–67.

[9] Couto C, Vila Real P, Lopes N, Zhao B. Resistance of steel cross-sections with local buckling at elevated temperatures. J Constr Steel Res 2015;109:101–14.

[10] Xing Z, Kucukler M, Gardner L. Local buckling of stainless steel plates in fire. Thin-Walled Struct 2020;148:106570.

[11] Xing Z, Kucukler M, Gardner L. Local buckling of stainless steel I-sections in fire: Finite element modelling and design. Thin-Walled Struct 2021;161:107486.

[12] Kucukler M. Compressive resistance of high-strength and normal-strength steel CHS members at elevated temperatures. Thin-Walled Struct 2020;152:106753.

[13] Theofanous M, Chan TM, Gardner L. Structural response of stainless steel oval hollow section compression members. Eng Struct 2009;31:922–34.

[14] ABAQUS. ABAQUS/standard user's manual. Version 6.17. Dassault Systemes Simulia Corp. USA; 2017.

[15] Fang H, Chan TM. Resistance of axially loaded hot-finished S460 and S690 steel square hollow stub columns at elevated temperatures. Structures 2019;17:66–73.

[16] Chan TM, Gardner L. Compressive resistance of hot-rolled elliptical hollow sections. Eng Struct 2008;30:522–32.

[17] Chan TM, Gardner L. Bending strength of hot-rolled elliptical hollow sections. J Constr Steel Res 2008;64:971–86.

[18] Gardner L, Chan TM, Abela JM. Structural behaviour of elliptical hollow sections under combined compression and uniaxial bending. Adv Steel Constr 2011;7: 86–112.

[19] Gardner L, Chan TM. Cross-section classification of elliptical hollow sections. Steel Compos Struct 2007;7:185–200.

[20] Ruiz-Teran AM, Gardner L. Elastic buckling of elliptical tubes. Thin-Walled Struct 2008;46:1304–18.

[21] Meng X, Gardner L, Sadowski AJ, Rotter JM. Elasto-plastic behaviour and design of semi-compact circular hollow sections. Thin-Walled Struct 2020;148:106486.

[22] Meng X, Gardner L. Simulation and design of semi-compact elliptical hollow sections. Eng Struct 2020;202:109807.

[23] Arrayago I, Real E, Gardner L. Description of stress-strain curves for stainless steel alloys. Mater Des 2015;87:540–52.

[24] Mirambell E, Real E. On the calculation of deflections in structural stainless steel beams: An experimental and numerical investigation. J Constr Steel Res 2000;54: 109–33.

[25] Rasmussen KJR. Full-range stress-strain curves for stainless steel alloys. J Constr Steel Res 2003;59:47–61.

[26] Gardner L, Ashraf M. Structural design for non-linear metallic materials. Eng Struct 2006;28:926–34.

[27] Chen J, Young B. Stress-strain curves for stainless steel at elevated temperatures. Eng Struct 2006;28(2):229–39.

[28] Gardner L, Insausti A, Ng KT, Ashraf M. Elevated temperature material properties of stainless steel alloys. J Constr Steel Res 2010;66(5):634–47.

[29] Gardner L, Bu Y, Francis P, Baddoo NR, Cashell KA, McCann F. Elevated temperature material properties of stainless steel reinforcing bar. Constr Build Mater 2016;114:977–97.

[30] Design Manual for Structural Stainless Steel, fourth ed., Steel Construction Institute (SCI); 2017.

[31] Ala-Outinen T, Oksanen T. Stainless Steel Compression Members Exposed to Fire, Research Notes 1864. Finland: Technical Research Centre of Finland (VTT); 1997.

[32] Afshan S, Zhao O, Gardner L. Standardised material properties for numerical parametric studies of stainless steel structures and buckling curves for tubular columns. J Constr Steel Res 2019;152:2–11.

[33] Rossi B, Degée H, Pascon F. Enhanced mechanical properties after cold process of fabrication of non-linear metallic profiles. Thin-Walled Struct 2009;47(12): 1575–89.

[34] Liang Y, Manninen T, Zhao O, Walport F, Gardner L. Elevated temperature material properties of a new high-chromium austenitic stainless steel. J Construct Steel Res 2019;152:261–73.

[35] EN 1993-1-5. Eurocode 3: Design of steel structures Part 1-5: Plated structural elements. European Committee for Standardization, Brussels; 2006.

[36] EN 10219-2, Cold formed welded Structural Hollow Sections Part 2: Tolerances, dimensions and sectional properties, European Committee for Standardization (CEN), Brussels; 2019.

[37] EN 10210-2. Hot-finished structural hollow sections Part 2: Tolerances, dimensions and sectional properties, European Committee for Standardization (CEN), Brussels; 2019.

[38] He A, Liang Y, Zhao O. Experimental and numerical studies of austenitic stainless steel CHS stub columns after exposed to elevated temperatures. J Constr Steel Res 2019;154:293–305.

[39] Tondini N, Hoang VL, Demonceau JF, Franssen JM. Experimental and numerical investigation of high-strength steel circular columns subjected to fire. J Constr Steel Res 2013;80:57–81.

[40] Qiang X, Bijlaard FS, Kolstein H. Elevated-temperature mechanical properties of high strength structural steel S460N: Experimental study and recommendations for fire-resistance design. Fire Saf J 2013;55:15–21.

[41] Kucukler M, Xing Z, Gardner L. Behaviour and design of stainless steel I-section columns in fire. J Constr Steel Res 2020;165:105890.

[42] Kucukler M. Cross-section stability and design of normal strength and high strength steel I-sections in fire. Int J Struct Stab Dyn 2022;2250146.

[43] AISC 360-16, Specifications for Structural Steel Buildings. American Institute of Steel Construction (AISC), Chicago; 2016.

[44] Young B, Hancock GJ. Tests of channels subjected to combined bending and web crippling. J Struct Eng ASCE 2002;128:300–8.

[45] Ziemian RD. Guide to stability design criteria for metal structures. 6th ed. John Wiley & Sons; 2010.

[46] Rotter JM, Sadowski AJ, Chen L. Nonlinear stability of thin elastic cylinders of different length under global bending. Int J Solids Struct 2014;51(15–16):2826–39.

[47] Xu Z, Gardner L, Sadowski AJ. Nonlinear stability of elastic elliptical cylindrical shells under uniform bending. Int. J. Mech. Sci. 2017;128–129:593–606.

[48] Martins AD, Gonçalves R, Camotim D. Numerical simulation and design of stainless steel columns under fire conditions. Eng Struct 2021;229.

[49] Gardner L, Chan TM, Wadee MA. Shear response of elliptical hollow sections. Proc Inst Civ Eng Struct Build 2008;161:301–9.

[50] Kempner J. Some results on buckling and post buckling of cylindrical shells. Collected papers on instability of shell structures. NASA TND 1962;1510:173–86.

[51] Gerard G, Becker H. Hand book of structural stability: Part III—Buckling of curved plates and shells. NACA Technical Note 1957::3783.

[52] Buchanan C, Gardner L, Liew A. The continuous strength method for the design of circular hollow sections. J Constr Steel Res 2016;118:207–16.

[53] McCann F, Fang C, Gardner L, Silvestre N. Local buckling and ultimate strength of slender elliptical hollow sections in compression. Eng Struct 2016;111:104–18.

[54] Abela JM, Gardner L. Elastic buckling of elliptical tubes subjected to generalised linearly varying stress distributions. Thin-Walled Struct 2012;58:40–50.

[55] McCann F, Gardner L. Numerical analysis and design of slender elliptical hollow sections in bending. Thin-Walled Struct 2019;139:196–208.

[56] Bock M, Gardner L, Real E. Material and local buckling response of ferritic stainless steel sections. Thin-Walled Struct 2015;89:131–41.

[57] Kruppa J. Eurocodes-Fire parts: proposal for a methodology to check the accuracy of assessment methods. Horizontal Group Fire, Document; 1999. p. 99–130. CEN TC 250,.

[58] Albero V, Espinos A, Romero ML, Hospitaler A, Bihina G, Renaud C. Proposal of a new method in EN 1994-1-2 for the fire design of concrete-filled steel tubular columns. Eng Struct 2016;128:237–55.

[59] Lopes N, Manuel M, Sousa AR, Vila Real P. Parametric study on austenitic stainless steel beam-columns with hollow sections under fire. J Constr Steel Res 2019;152: 274–83.

[60] Couto C, Coderre T, Vila Real P, Boissonnade N. Cross-section capacity of RHS and SHS at elevated temperatures: comparison of design methodologies. Structures 2021;34:198–214.

[61] dos Santos GB, Gardner L, Kucukler M. A method for the numerical derivation of plastic collapse loads. Thin-Wall Struct 2018;124:258–77.

[62] Quan C, Kucukler M, Gardner L. Out-of-plane stability design of steel beams by second-order inelastic analysis with strain limits. Thin-Walled Struct 2021;169: 108352.

[63] Fieber A, Gardner L, Macorini L. Design of structural steel members by advanced inelastic analysis with strain limits. Eng Struct 2019;199:109624.

[64] Lee SC, Lee DS, Yoo CH. Flexure and shear interaction in steel I-girders. J Struct Eng ASCE 2013;139:1882–94.